Calibration and 3D Model Generation for a Low-Cost Structured Light Foot Scanner

by

Navaneetha Kannan Viswanathan

A thesis
presented to the University of Waterloo
in fulfillment of the
thesis requirement for the degree of
Master of Applied Science
in
Mechanical Engineering

Waterloo, Ontario, Canada, 2012

AUTHOR'S DECLARATION

I hereby declare that I am the sole author of this thesis. This is a true copy of the thesis, including any required final revisions, as accepted by my examiners.

I understand that my thesis may be made electronically available to the public.

Abstract

The need for custom footwear among the consumers is growing every day. Serious research is being undertaken with regards to the fit and comfort of the footwear. The integration of scanning systems in the footwear and orthotic industries have played a significant role in generating 3D digital representation of the foot for automated measurements from which a custom footwear or an orthosis is manufactured. The cost of such systems is considerably high for many manufacturers due to their expensive components, complex processing algorithms and difficult calibration techniques.

This thesis presents a fast and robust calibration technique for a low-cost 3D laser scanner. The calibration technique is based on determining the mathematical relationship that relates the image coordinates to the real world coordinates. The relationship is determined by mapping the known real world coordinates of a reference object to its corresponding image coordinates by multivariate polynomial regression. With the developed mathematical relationship, 3D data points can be obtained from the 2D images of any object placed in the scanner.

An image processing script is developed to detect the 2D image points of the laser profile in a series of scan images from 8 cameras. The detected 2D image points are reconstructed into 3D data points based on the mathematical model developed by the calibration process. Following that, the output model is achieved by triangulating the 3D data points as a mesh model with vertices and normals. The data is exported as a computer aided design (CAD) software readable format for viewing and measuring.

This method proves to be less complex and the scanner was able to generate 3D models with an accuracy of +/-0.05 cm. The 3D data points from the output model were compared against a reference model scanned by an industrial grade scanner to verify and validate the result. The devised methodology for calibrating the 3D laser scanner can be employed to obtain accurate and reliable 3D data of the foot shape and it has been successfully tested with several participants.

Acknowledgements

I would like to offer my sincere gratitude to my supervisors, Dr. Jan Huissoon and Dr. Sanjeev Bedi for supporting me throughout my thesis with patience and knowledge. I attribute the level of my Masters degree to their encouragement and effort. Special thanks to Tezera Ketema for his strong motivation and trust on me and this research.

I am thankful to Professor. Naveen Chandrashekar and Professor. Behrad Khamesee for agreeing to read my thesis and for their valuable feedbacks towards the betterment of the thesis. I would like to acknowledge Dr. Jonathan Kofman and Luigi Giaccari for sharing their knowledge and expertise in computer vision systems and surface reconstruction.

I must also mention my gratitude to Sam Lochner for his friendly assistance and encouragement throughout this journey. Special thanks to Dragos Besliu, Vinodhkumar and Sudipto Dolui for their assistance in the laboratory.

I would like to thank my friend Teja Vajha for the many hours spent in the experiments and for his priceless support and assistance. Finally, I thank my parents and my sister for their love and moral support although I was miles away from them.

Dedication

To my Motherland and Manju

Table of Contents

List of Figures

List of Tables

Chapter 1
Introduction

The footwear industry serves billions of people across the globe every year and satisfying the needs of every consumer has become an essential goal for the industry. The diverse industry produces numerous varieties of everyday footwear for men, women, children as well as specialized products like winter boots, athletic footwear, and protective footwear. The footwear industry remains a highly specialized and competitive environment as it aims to satisfy consumers in terms of fitness and comfort. Most footwear manufacturers need to be as efficient as possible while providing high quality footwear for the majority of customers. In recent years, this drive for efficiency has increased due to the rise in international trade and competition as well as increased consumer demand. As a result, footwear manufacturers have found it crucial to adapt to the market conditions by providing footwear with a wide variety of styles and sizes. Lately, the integration of computers and automation in the footwear industry has been relatively limited compared to other fields due to the high costs of setup and complex computations involved.

The research presented in this thesis focuses mainly on the software development for a proof-of-concept three dimensional foot scanning system for custom shoe manufacturing. The scanner presented in the thesis provides a solution to this need for improved productivity and efficiency due to its low cost and reliable output.

1.1 Project Motivations

The following section reviews the shoemaking process and the role of optical scanning systems in the footwear industry. The applications of two dimensional and three dimensional scanning systems for integrated footwear manufacturing and custom orthoses are also discussed to understand the demand for such systems.

1.1.1 Shoe making

A typical shoe maker starts the job with a last made traditionally from wood, but now often made of plastic as shown in Figure 1-1. The design of the last represents the shape and measurement of the customer's foot. These measurements for the last are acquired through measuring sticks, measuring tapes and calipers. The last is then used to cut the upper materials and the sole of the shoe. Following that, the last is removed after the upper materials and the sole are sewn and nailed together. It is naturally a tedious work to develop a last for each customer the shoe maker has to deal with. As a result, the shoe lasts are typically made from a generic template and are pre-crafted for various common sizes.

For un-common sizes or cases with some artifacts, new lasts are custom made. With the help of a last, a mock shoe is made as per the quality and aesthetic requirements of the customer. The mock shoe is then tested by the customer for fit and comfort. If necessary, the required changes are made in the last and then the shoe is finally crafted.

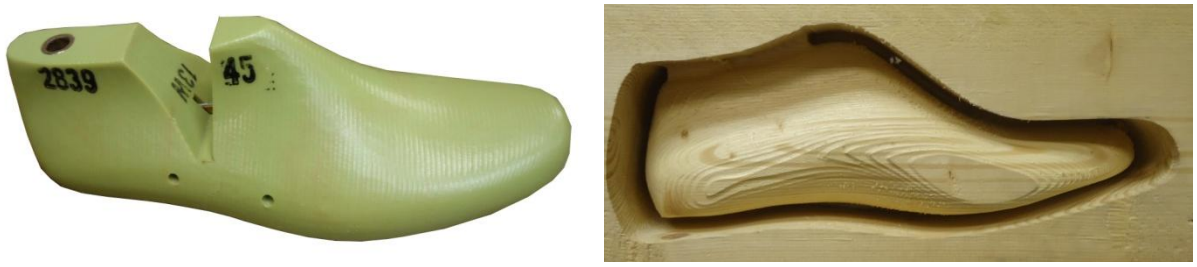

Figure 1-1 Plastic and wooden shoe last

Since the process involves a lot of manual measurements, errors are significant. The entire process of measuring, computing and manufacturing is laborious and time consuming. In addition, since the foot measurement data is not common among manufacturers, the customers are constrained to approach the same manufacturer each time they need new footwear.

On the whole, the process of shoemaking can be classified into two major types (as shown in Figure 1-2); conventional or traditional methods of manufacturing and custom manufacturing.

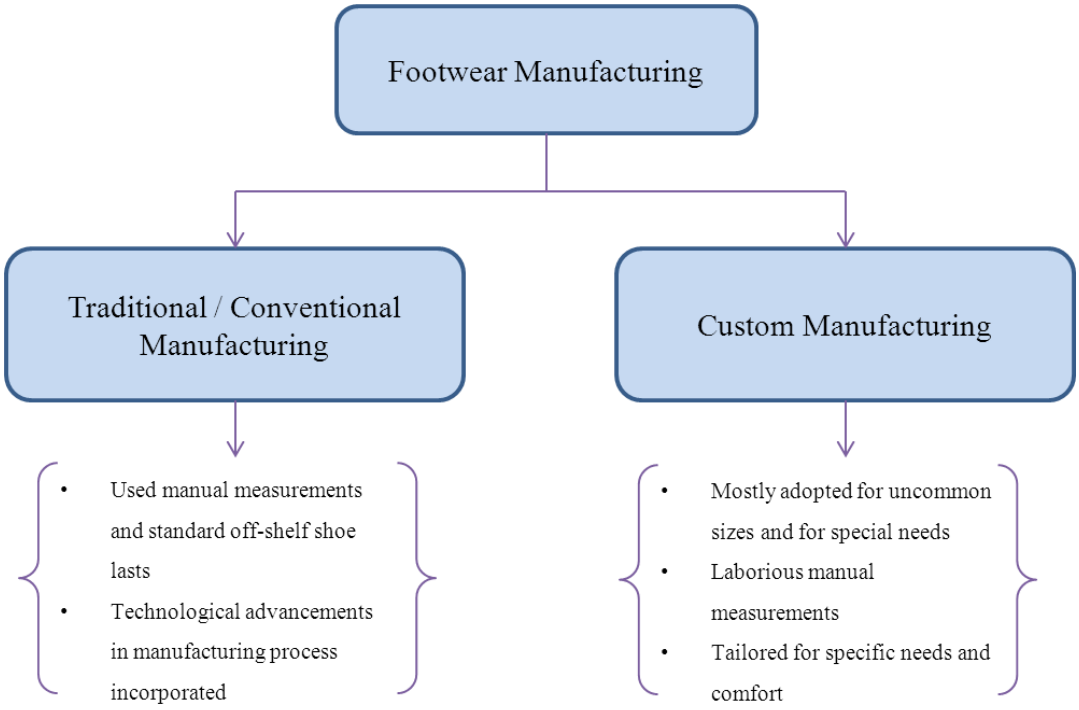

Figure 1-2 Generic classification of footwear manufacturing

While the custom footwear manufacturing industry had to rely on the conventional manual process; commercial and mass manufacturing industry began to use the benefits of technological advancements in automated manufacturing. The use of injection molding techniques, CNC based last milling, pattern cutting and sewing had tremendous impact in optimizing the commercial shoe manufacturing process.

Due to the absence of technological advancements in foot measuring techniques, custom manufacturing has become relatively expensive in terms of time and cost. On average, a custom shoe maker charges about two to three thousand dollars for a custom shoe and takes nearly 4 hours to manufacture a last for the same [1]. So, any development or break-through in the process of measurement and last manufacturing would drastically bring down the overall time.

Advancements in scanning systems have proven useful for obtaining a computerized model of a foot. Figure 1-3 shows a c \onceptual flow diagram of a foot wear manufacturing system integrated with a scanning system. This typically eliminates the laborious work involved in measuring the foot with calipers, measuring sticks and measuring tapes. Hence, with the help of scanning systems, foot measurements can be taken with ease and drastically reduce the manual error. This potential blend of technology has developed an interest in the footwear and orthoses manufacturing industries to adopt and stand-out in delivering products with a good fit and comfort for the customers.

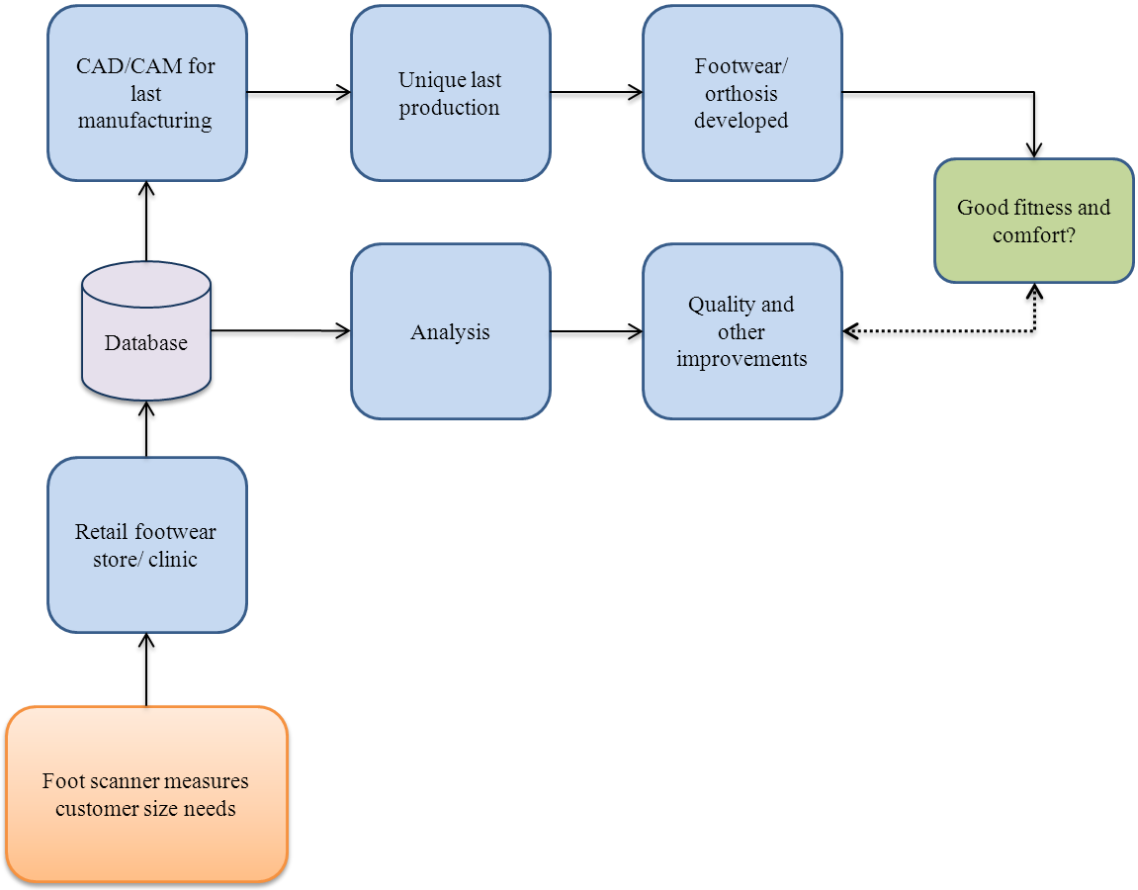

Figure 1-3 Schematic flow of footwear manufacturing integrated with a scanning system

Although the integration of scanning systems in the footwear and the orthosis manufacturing industries has many advantages, the high cost of implementing such systems in a retail store or a

clinic is still the biggest disadvantage. For example, a three dimensional foot scanning system in the market costs in the range of $ 25,000 to $ 75,000 (Canadian dollars). Since only a few retailers can afford to purchase such a scanning system, the majority of the retailers are in need of a low-cost scanning system that suits their needs.

1.2 Current Research

As mentioned earlier, the research mainly focuses on the software developed for the scanning system to digitize the foot and generate a measurable three dimensional CAD model using a fast and reliable optical calibration technique. This enables last manufacturing in a shorter period of time and more importantly without any human errors that result from manual methods. The CAD file of the foot data can be easily shared and accessed through the internet which makes it easy for the consumer to order footwear or make medical consultations with the click of a mouse. Also, for the orthotics industry and foot clinics, the CAD file could be used by clinicians or practitioners to access the patient's foot data on their computer without the physical presence of the patient.

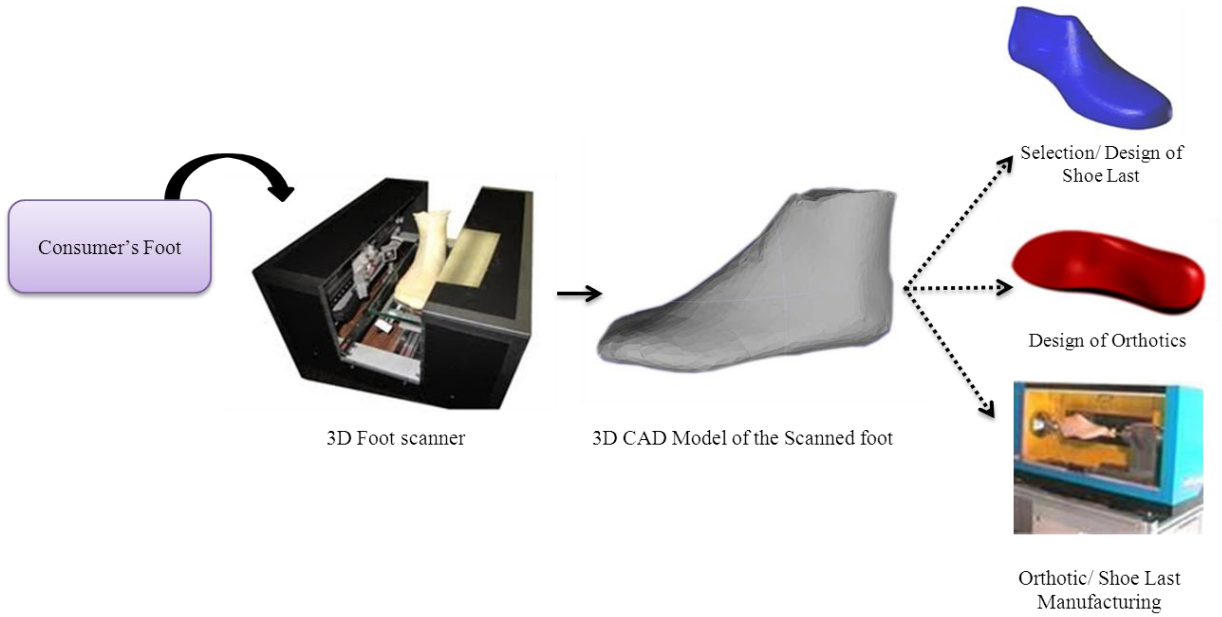

Figure 1-4 Research motive and Scope

1.3 Earlier Work

Prior to the research presented in this work, a 2D scanning system to produce a plantar shoe surface was designed and deployed [1]. A brief overview of the system is presented in this section. The result of the deployed 2D scanner inspired and motivated the development of a 3D scanning system that could digitize the foot and produce a CAD model.

The first basic measurement step of a shoe maker is to start by tracing the perimeter of the foot, from which the contours and sizing can be estimated. This preliminary measurement can be easily made with a simple 2D scanning system, involving a camera and acquisition hardware. This method enables capturing of the subject data with more accurate information on features and landmarks. This has a significant impact in the making of plantar shoe surface. A step further, integration of CAD/CAM with this system proves to be advantageous. As a result, an automated system for custom orthotic sandals with a series of 2D scan images has been developed [2].

To stress the significance of the advantage of 2D scanning, the following is a brief insight on the research done by Lochner [1] towards the development of custom orthotic sandal from 2D scan images. The plantar regions of left and right foot of the customer are acquired by an off the shelf 2D scanner. The acquired images are uploaded to a processing server, which enables the operator or clinician to choose points on the image manually in order to estimate the length and width of the foot. Additionally, key features like toe crest, ball joint and other distinct features can also be identified and noted.

Once the landmarks are identified, programmed scripts would run the automatic contouring of the foot. The images are placed in a 3D space where a custom orthotic is extrapolated with the Rhino API script.

This research, with the help of an industrial partnership was applied to commercially manufacture custom orthotic sandals. The CAD extrapolated sandal sole was then manufactured using ethylene vinyl acetate material in a CNC mill. Following that, sole covers and upper straps are added to make the finished product.

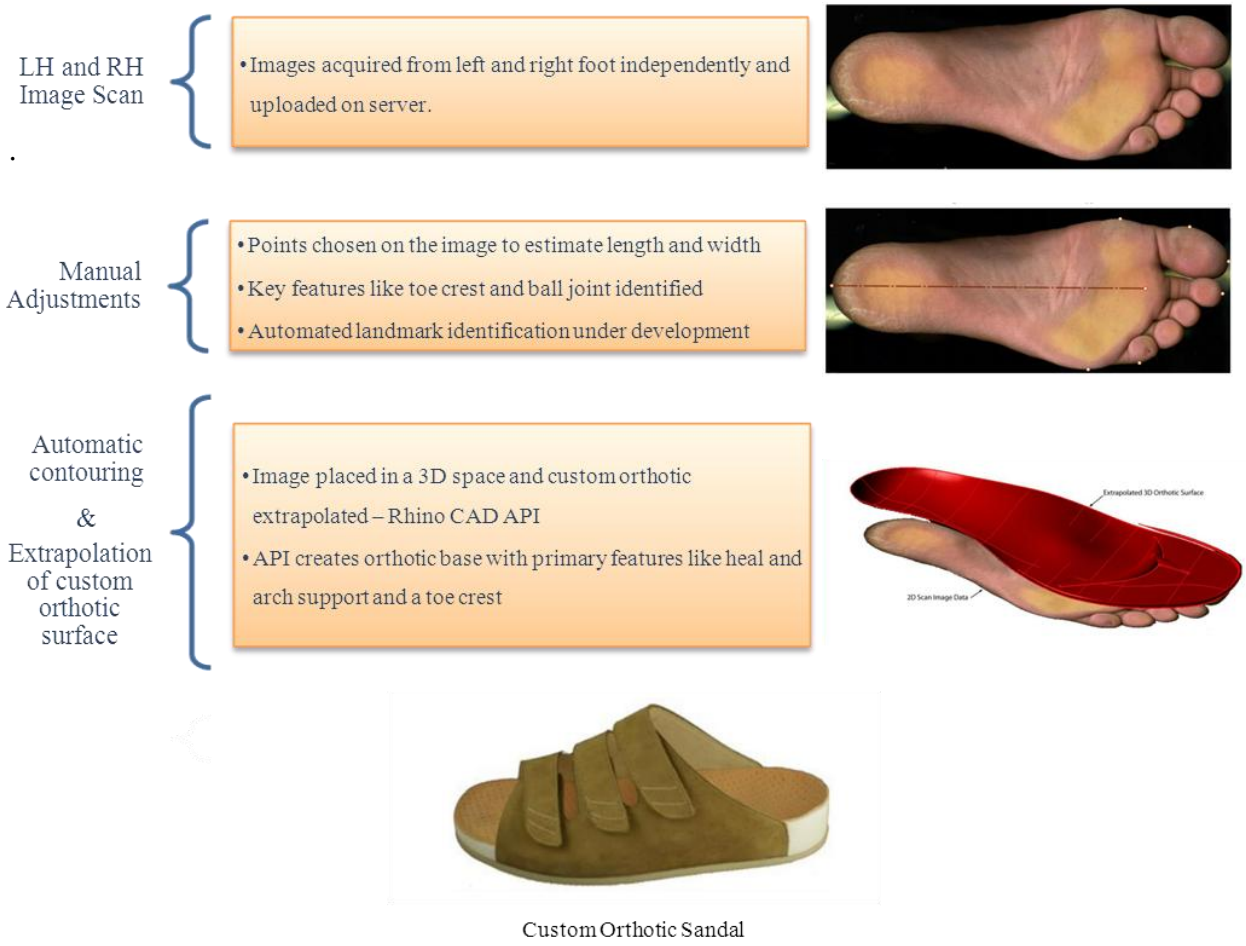

Figure 1-5 Two-dimensional scanner for custom orthotic sandal developed at the University of Waterloo [1, 2]

1.4 Thesis Layout

The remainder of this thesis has the following layout.

Chapter 2 reviews the study of basic foot geometry, optical scanning methods, calibration techniques of cameras and insight on three dimensional laser scanning systems.

Chapter 3 describes the three dimensional laser scanner devised to digitize the foot. Also, various criteria and considerations are discussed in detail.

A detailed discussion on calibrating the laser scanner is presented in Chapter 4. Following that, Chapter 5 presents the implementation and working of the laser scanner more elaborately. Chapter 6 presents the performance verification and results and Chapter 7 presents the conclusion, recommendations and future work to be carried out in the system.

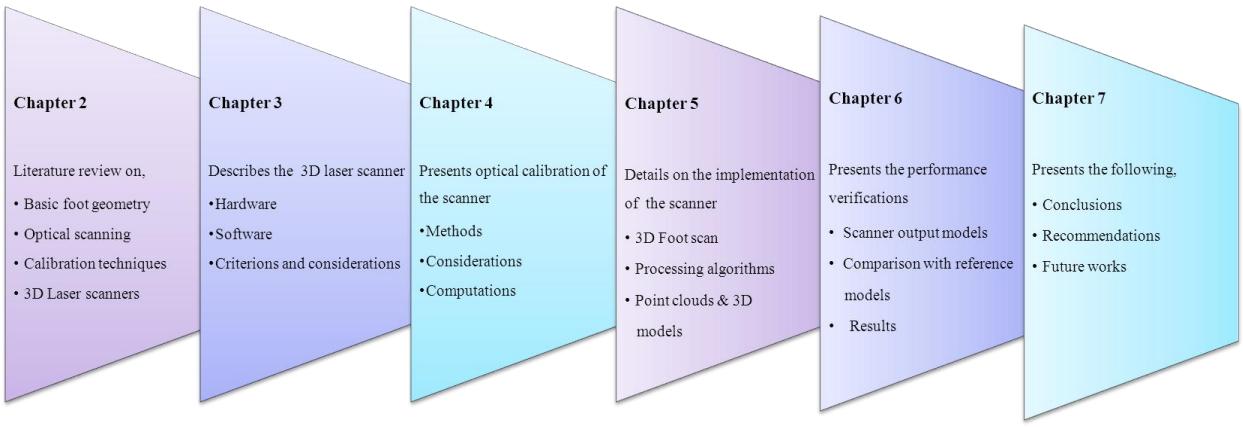

Figure 1-6 Thesis organization

Chapter 2
Literature Review

2.1 Overview

Computer vision and scanning systems have witnessed numerous improvements and innovations in the field of shape measurements. This chapter of the thesis is intended to familiarize the reader with four major segments that are essential for understanding 3D foot scanning techniques. The first segment guides the reader through the basic foot geometry measurements essential for shoe last or custom orthoses manufacturing. The second and third segments elaborate on various optical scanning techniques applied to 3D object measurement and calibration methodologies for cameras used in the scanning system. The 3D laser scanning technique is discussed in detail in greater fourth segment of this chapter.

2.2 Basic foot geometry measurements

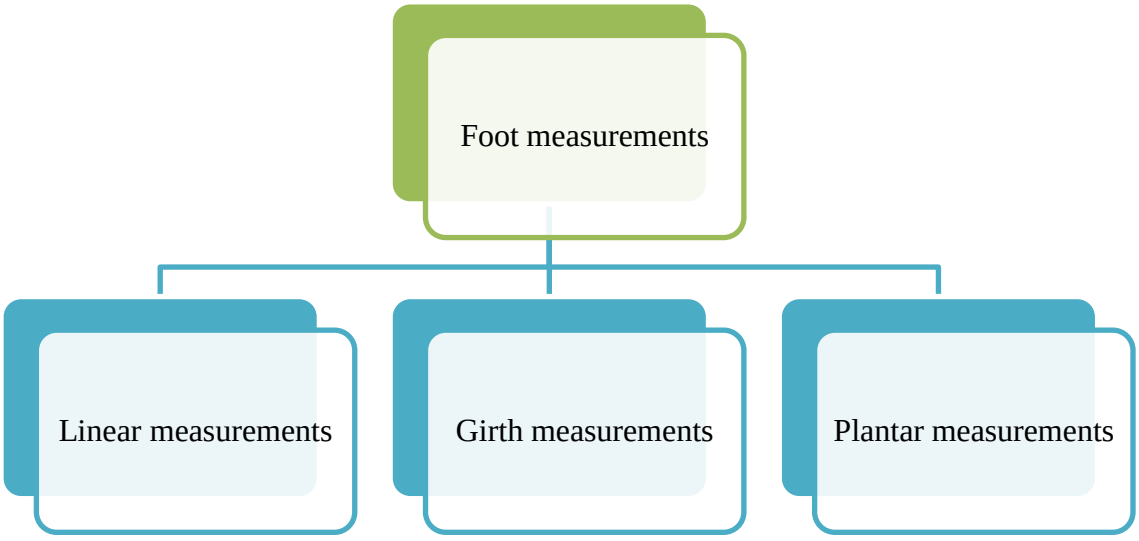

Figure 2-1 Generic classification of foot geometry measurements

2.2.1 Linear Measurements

The most common foot measurement taken by a shoemaker or a retailer is the length of the foot, with which the customers are given the closest fitting shoe off the shelf. These sizes are regulated and defined by various national and continental sizing systems [3]. Depending on the need/retailer/shoemaker/demography, the method of measurements is carried out. For example, use of a Brannock device (shown in Figure 2-2) helps in measuring the length, the width and the arc length of the foot.

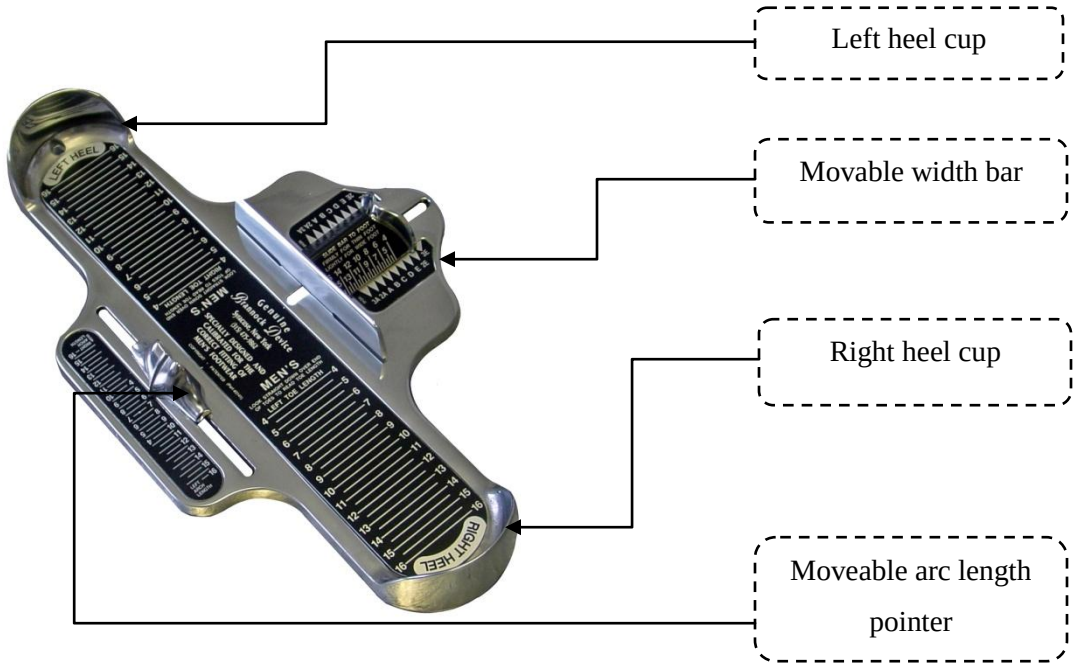

Figure 2-2 Brannock device [4]

Witana et al. [5] and Liu et al. [6] present various methodologies for generating foot measurements from a 3D scan data. The former used the 3D shape of the foot from a high-end 3D scanning system that could generate 3D surface data along the length of the foot. Based on the linear measurements, Krauss et al. [7] categorizes the human feet into different types: voluminous, flat-pointed and slender. Various studies have been carried out to validate the results of linear measurements obtained by

automated measurements to be in line with the results of earlier studies based on manual measurements. Lou et al. [8] applied the 3D scanning technique to assess the differences in foot shape with gender. The results were proven to be in line with the earlier study made by Wunderlich et al. [9].

2.2.2 Girth Measurements

A step further to linear measurement of the foot, it was found necessary to have a detailed data on the overall foot shape to manufacture shoe lasts (as discussed earlier in chapter 1). Development of shoe lasts generally needs in depth foot measurements of the customer's foot so as to manufacture footwear with a good fit and comfort. Bao et al. [10] presented an integrated system for manufacturing custom shoe lasts for the orthopedic shoe design. Witana et al. [5] and Nacher et al. [11] used 3D scanners with girth measurement algorithms to measure the non-contact areas (due to the irregular shape of the foot) and also investigated the quality of fit between the foot and shoe based on the computed measurements. Wang [12] scanned 10 shoe lasts and developed a process for selecting a last that would most suit for the individual based on various girth measurements like ball girth, waist girth and instep girth of the foot.

2.2.3 Plantar Shape Measurement

Similar to linear and girth measurements, a lot of research has been carried out specifically in measuring the plantar surface of the foot. This measurement is considered to be vital for any custom orthosis manufacturing. It is proven that customers with custom orthosis enjoy a good fit and comfort than preferring an off the shelf orthosis. Hawke et al. [13] conducted clinical trials and evaluated the effectiveness of custom orthotics. Over the past decade, a large number of 2D scanning systems to measure the plantar surface have evolved in the market.

Modern surface scanning techniques is integrated with the software packages to enable fast and reliable orthosis design. Some notable software packages include, Orthomodel from Delcam PLC, UK and PlantarScan, Precision 3D, UK.

An alternative method for obtaining the shape of the foot rather by casting or scanning is the impression foam system [14]. The patient is made to stand with their foot pushed into a low density foam box. As the foam collapses with the self-weight, a negative of the foot shape is achieved. The box is either filled with plaster or scanned directly to obtain the positive cast.

2.2.4 Dynamic Measurements

The advancements in optical technologies provided ways to measure dynamic changes in foot shape during walking and other actions [15]. The process is highly computational because of its complexity and is expensive. Kimura et al. [16] uses 12 video cameras and a walkway for the study of dynamic changes. Jezerek et al. [17] uses the multiple-laser-plane triangulation to measure the 3D geometry. Recent advancements in this method include the pressure mapping and pin device systems to analyze the variations in foot shape during various actions.

The extensive use of optical scanning systems is evident from the above study. The traditional manual measurements are slowly being replaced by the advanced optical scanning instruments. The following section presents a detailed study on various optical scanning methods for 3D shape measurements.

2.3 Optical Scanning methods

In the current industrial scenario, there is a need for accurate measurement of 3D objects to enhance the speed of a product development along with the quality of manufacturing [18]. This technology is more prevalent in reverse engineering, part inspections, dimension measurements, intelligent robots, and obstacle detection for vehicle guidance.

With the rise of technological advancements in computer technology integrated with digital scanning systems, 3D measuring systems/scanners have become commercially successful. Another major advantage of these optical scanners is that it allows non-contact based measurement with a high accuracy and denser data points, which carves the way for more research and analysis based on the output data. The cost of such scanning systems becomes expensive due to the sophisticated optical and electronic setup.

There have been many efforts to reduce the cost of a commercial foot scanner. Blais et al. [19] designed 3 optical sensors to reduce the cost of foot scanner. Kouchi et al. [20] applied the concept of homologous shape modeling and Leon Kos [21] introduced automatic landmark detection algorithm to design a low cost foot scanner that generates a customized shoe last based on the extracted foot shape.

However the cost of these scanners is still too high to be used in a conventional retail store/clinic, as these scanners still implement the 3D measurement technique with expensive hardware setup.

2.3.1 Optical 3D Measurement Techniques

Over the past few years, a wide range of optical techniques have been applied to measure a 3D shape. Figure 2-3 illustrates the generic classification of the 3D measurement techniques and a brief overview of these techniques discussed in [22] is reviewed in this section of the thesis.

3D Measurement by Optics	Time/light in flight
	Laser speckle pattern
	Moiré method
	Interferometry
	Photogrametry
	Structured light
	Laser scanning

Figure 2-3 Three dimensional measuring techniques by optics [22]

2.3.1.1 Time/Light in flight

Time of flight based method of 3D measurement is based on estimating the depth information by measuring the duration of flight of a light source from a source point to the receiver point [23]. During the measurement, the object pulse is reflected back to the receiver and is compared with the reference pulse for the time difference. This difference is mathematically related to the distance. The resolution of the device operating with this method purely depends on the high resolution electronics and the pulse generation time [18]. This technique serves as the basic principle of operation for laser range finders.

2.3.1.2 Laser speckle pattern sectioning

This method is purely based on the transformation relationship between the optical wavelength/frequency space and the distance/range space to measure the shape of an object [24, 25, 26]. A speckle pattern is acquired and measured using a CCD array at various laser wavelengths, and the individual frames are aggregated to generate a 3D data array. Following that, a 3D Fourier transform is applied to this data array to obtain the 3D shape of an object. Some major advantages of this technique are (1) the high flexibility of measurement range and (2) that it does not require phase

shifting as in the case of conventional interferometry. The time to acquire images with different wavelengths was found to be too long for relatively large scale shapes and hence it is not preferred in the industry [18].

2.3.1.3 Moiré method

The Moiré method can be divided into a projection of light and the shadow based method of measurement. Takasaki[27] and Harding et al. [28] have elaborated more on the Moiré topography and the application of Moiré method in visual inspection of machined parts . The technique uses two gratings, namely a master grating and a reference grating, from which contour fringes can be generated and resolved by a charge coupled device (CCD) camera. The Logic-Moiré method discussed in [29, 30] employs a computer generated reference grating and a computer resolved master grating. The complexity in construction, time and implementation becomes the drawback in industrial and commercial applications. To overcome this drawback, various studies have been carried out and use of multiple image fringe patterns with different phase shifts were then introduced to overcome the environmental perturbations and to reduce the process time [18]. The comparison of high speed Moiré methods, applications and related references can be found in [18, 31].

2.3.1.4 Interferometry

The basic idea behind interferometry based shape measurements is the formation of fringes by varying the sensitivity matrix (usually controlled by computer) that relates the geometry of the scanned object to the measured optical phases. The key variables of the sensitivity matrix are the wavelength, refractive index and the illumination and direction of observation. Dalhoff et al. [32] presented the double heterodyne interferometry using a frequency shift technique to measure 3D shapes of high accuracy with 0.1mm resolution . It was also proven in the same research that the integration of phase shifting technique with the interferometric method and the heterodyne technique

can have accuracies of 1/100 and 1/1000 of a fringe respectively. Some of the advanced methods of Interferometry include, shearography, diffraction grating, digital wave front reconstruction and wave length scanning and conoscopic holography [48].

2.3.1.5 Photogrammetry

Photogrammetric 3D reconstruction technique employs the bundle adjustment principle, where the geometric model and the orientation of the bundles of light rays in a photogrammetric relationship is developed analytically and is implemented by the least squares procedure [34]. It typically uses one of the stereo techniques, defocus, shading or scaling to measure the 3D shape. Photogrammetry is primarily used in the feature type 3D dimension measurement. It is carried out by having bright markers on the surface of the object being measured. Extensive research has been carried out by Fraser [35] to improve the accuracy of this method and proved to have high accuracy as one part in 100,000 or even one part in 1,000,000.

2.3.1.6 Structured light

Structured light method is another commonly used method to obtain the 3D surface geometry of the scanned object. It employs a projected coded (mostly binary coded) light and a sinusoidal fringe technique. The depth information of the 3D object is encoded into a deformed fringe pattern and is captured by the image acquisition sensor [18]. Structured light based measuring systems are advantageous due to their ease of implementation and few moving parts. Moving parts in a scanning system have significant effect on the accuracy of the measurements. In this case, computer controlled structured light scanning systems eliminates moving parts and that helps phase shifting, fringe density and directional changes to be more precise and accurate, leading to highly accurate measurements. Due to these advantages the structured light based scanning systems have become commercially successful, despite the issue of shading problem. Also, the scanning system is vulnerable to ambient

light and becomes challenging to handle in a brighter environment. Some of its common applications are discussed in [36].

2.3.1.7 Laser Scanning

Laser scanning technology is a well-known and is the most employed 3D measurement technique. It utilizes the triangulation relationship in optics to establish the 3D data/shape of the scanned object. Moreover due to its ease of construction and application of mathematical models is more pertinent to the current industrial needs. The typical measurement range is +-5 to +-250 mm and accuracy is about 1 part in 10,000 [37, 38]. The basic construction of laser scanners includes a laser and a charge coupled device (CCD), or a position sensitive detector (PSD) to digitize the laser range images.

The measurement accuracy (if in case of a PSD) mainly depends on the accuracy of the image formed on the image sensor and also the reflection of beam spot/stripe. The ambient light penetrating the system was found to be one of the major causes in loss of accuracy in these systems. Idesawa [39] developed methods to improve the accuracy of PSD with the use of the high accuracy kaleidoscopic mirror tunnel position sensing technique and a hybrid PSD. Another major factor that accounts for the accuracy of a laser scanning system is the effectiveness of calibration. Chapter 2.4 discusses more on the various calibration methods that can be used and their impact on the scanning system in detail. The measurement accuracy also depends on the difference in surface characteristics of the measured object and the calibration object. Ideally, calibration should be performed on similar surfaces to ensure the measurement accuracy. With the well-made calibration setup for the laser scanners, it is possible to directly measure the 3D coordinates of a large number of points in a very short period of time. It also enables the RGB values for each pixel in the image to be obtained, which proves to be valuable in applications like texture mapping of the scanned model/shape and scene reconstruction.

2.4 Calibration techniques

The primary objective of calibration is to establish the projection from the 3D world coordinate system to the 2D image coordinate system. With a known projection, 3D information can be inferred from the 2D images acquired the by the laser scanner's acquisition device. Zhang [40] classifies the camera calibration techniques into two main categories: Reference-object based calibration and Self-calibration.

2.4.1 Self-calibration and Reference-object based calibration

2.4.1.1 Self-calibration

This method of calibration involves recovering the intrinsic and the extrinsic parameters of a camera. Figure 2-4 illustrates the classification of camera parameters and its brief description.

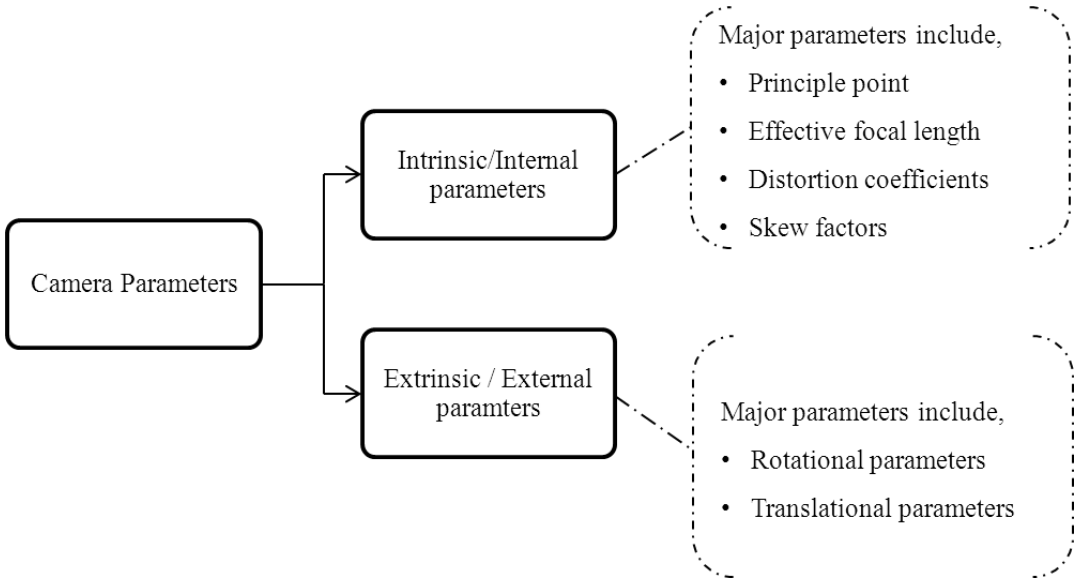

Figure 2-4 Classification of the camera parameters

The intrinsic parameters, also known as the internal parameters, determine the projective behavior of the camera, while the extrinsic parameters determine the mapping from the real world coordinates to the camera coordinate system [41, 42].

- The intrinsic parameters of a camera include the details on principle point, effective focal length, and distortion co-efficient and skew factor. The principle point of a camera is a point where the optical axis coincides with the image plane or the image-sensor plane of a camera. The effective focal length ' f ' of camera is defined in two values along x-axis and y-axis, namely, ' f_x ' and ' f_y '. Distortions in a camera are due to the optical aberrations in the lens of the camera [42]. The skew factor of the camera is defined as the angle between the pixels in the x-axis and y-axis respectively. Imperfections in manufacturing are the main source of this factor.
- The extrinsic parameters of a camera include three rotational parameters and three translational parameters. The rotational parameters of a camera give the orientation of the camera coordinate system in the world coordinate system, while the translation parameters relate the origin of the camera coordinate system in the world coordinate system [42].

2.4.1.2 Reference object –based calibration

The camera calibration process is accomplished by observing a calibration object of precisely known geometry in 3D world space. Usually the calibration object consists of two or three planes orthogonal to each other in order to effectively extract the depth information from a 2D image.

2.4.2 Single camera calibration

With the images from camera of known internal parameters, correspondence between three images can be used to recover internal and external parameter which allows in reconstructing 3D models [40].

Clarke et al. [43] presented a detailed review of widely used camera models and calibration techniques. The most commonly used camera model is the pinhole model. Various pinhole model

based algorithms for camera calibration are presented in [40, 44, 45]. In those models, the camera is assumed to perform a perfect perspective optical transformation. Figure 2-5 illustrates the pinhole camera model.

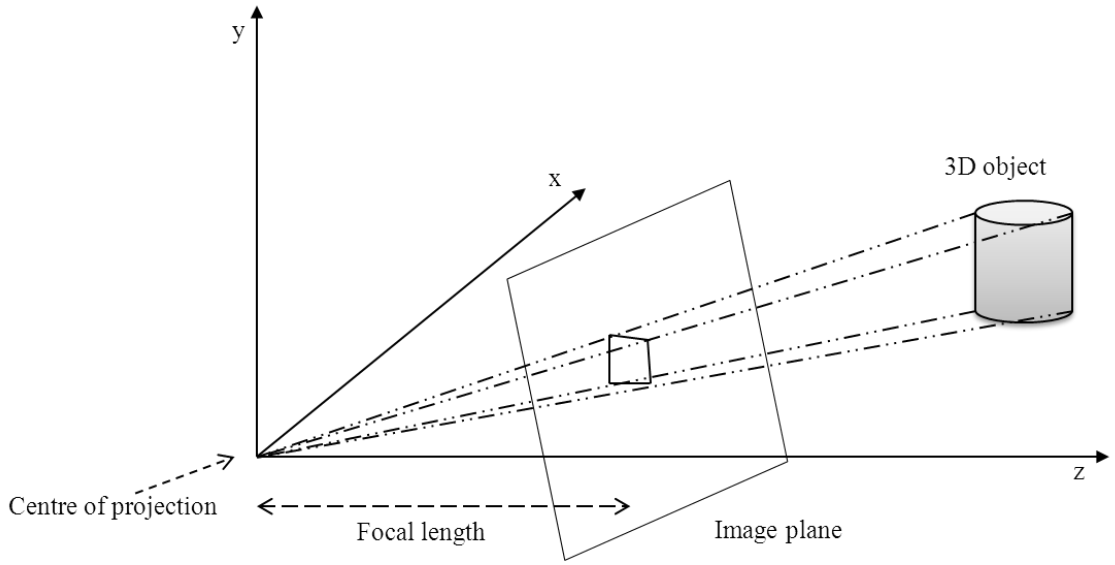

Figure 2-5 Pinhole camera model

The mapping from image coordinates to world coordinates can be written as [40]:

$$sm = A[R \mid T]M \tag{2.1}$$

or, expanded as,

$$s\begin{bmatrix} i \\ j \\ 1 \end{bmatrix} = \begin{bmatrix} f_x & 0 & c_x \\ 0 & f_y & c_y \\ 0 & 0 & 1 \end{bmatrix} \begin{bmatrix} r_{11} & r_{12} & r_{13} & t_1 \\ r_{21} & r_{22} & r_{23} & t_2 \\ r_{31} & r_{32} & r_{33} & t_3 \end{bmatrix} \begin{bmatrix} X \\ Y \\ Z \\ 1 \end{bmatrix} \tag{2.2}$$

Where (X, Y, Z) are the 3D real world coordinates, (i, j) are the image coordinates. The image plane is shown ahead of the projection center for better visualization and understanding, although it is actually behind. In equations 2.1 and 2.2, 'A' represents the camera matrix, c_x, c_y are the principle

points along x and y directions respectively. f_x and f_y are the focal lengths in x and y directions respectively, expressed in pixel units. The joint rotation-translation matrix R|T is usually known as the extrinsic matrix and describes the pose of the image plane in the camera to the real world coordinates [41]. To consider lens distortion in the calibration process, parameters k_1, k_2 are introduced to determine the radial distortions and p_1, p_2 for the tangential distortions. Tsai [47] mentions that only radial distortion plays a significant role in machine vision applications.

The calibration techniques are usually based on known space coordinates/ geometry of a calibration object (as mentioned in section 2.4.1.2). The calibration objects employed to recover the camera parameters can be either a 2D [47] or a 3D [48] or a planar [40] object. The calibration method presented in [40] uses a 2D planar calibration grid, which is placed at different positions and orientations in front of the camera. The feature points of the planar checkerboard pattern are extracted by image processing and the projective transformation between the image points of different images and the corresponding 3D points are computed. Figure 2-6 shows a 7x6 checkerboard pattern.

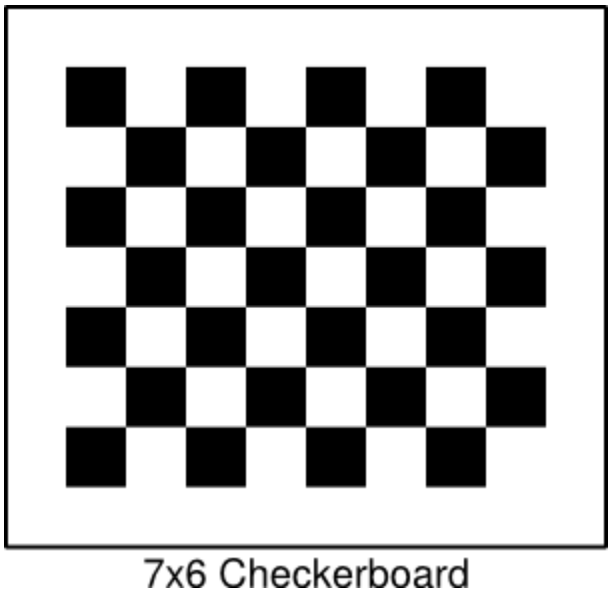

Figure 2-6 Checkerboard pattern to determine the camera parameters

The camera's intrinsic and extrinsic parameters are computed next by direct linear transformations. Following to that, the radial distortion terms are computed by linear least squares and the re-projection errors incurred in the process are minimized by using the Levenberg-Marquardt method [49, 50].

2.5 3D Laser Scanners

As mentioned earlier in section 2.3.1.7, the 3D laser scanners are currently the pick among all the other scanning systems, because of their high accuracy and precision with a low processing time. Primarily, a laser scanner employs a laser diode, a capturing device (CCD or PSD) and a processing system to acquire range images of the scan object in order to process the 2D images into 3D data points. Extensive research has been carried out in this field of scanning systems to improve the accuracy and precision of the output results. Improvements in the field of digital acquisition systems have carved a way to much advancement in 3D laser scanning systems.

For example, increments in the frame grabbing rate of CCD cameras, usage of sophisticated PSD devices and the development of smart sensors [50] that could produce 1000 images per second are a few notable advancements in 3D laser scanning systems.

Telfer et al.[3] splits the technology of producing a 3D representation of a foot into two categories: scanners and digitizers. Scanning is a process where 3D images are converted to digital form using the optical setup; and digitizing involves tracing of a 3D object's features and digitally stored on a computer [3]. But, in modern systems, the line between the mentioned two methods has become somewhat blurred and no particular distinction was drawn between the foot scanners using the differing approaches.

Forest et al.[51] classifies the approach of 3D measurements and reconstruction using laser digitizers based on raw acquisition, space encoding and smart sensor based. The proposed classification gives a

detailed understanding on the laser scanning 3D digitizers. A brief overview on the understanding is summarized in the following section.

2.5.1 Generic Classification

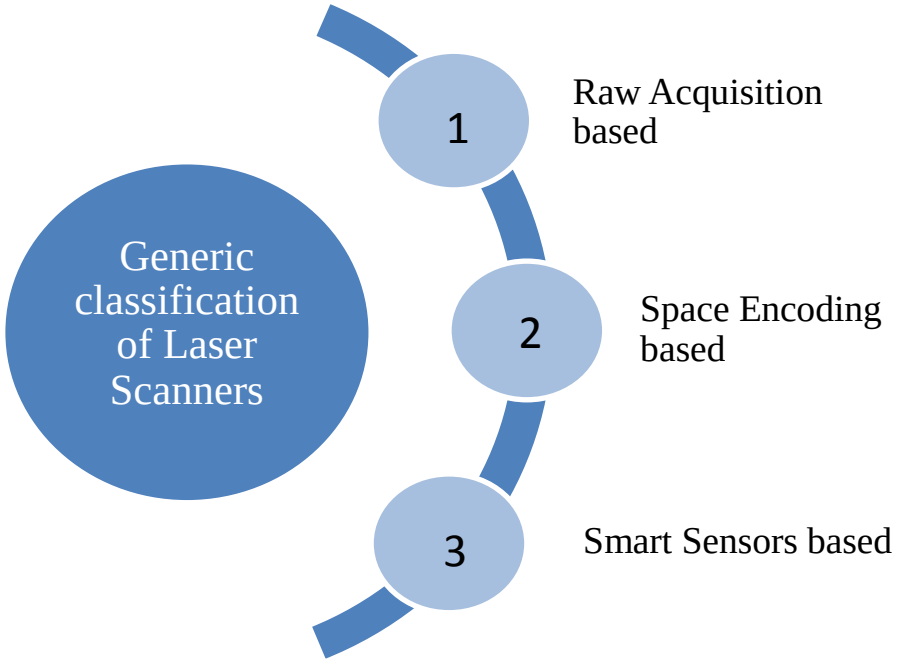

Figure 2-7 Classification of 3D laser digitizers [51]

2.5.1.1 Raw Acquisition

The basic approach of acquiring a range image from image acquisition hardware once the laser beam is passed on to the scene is widely known as raw acquisition. The number of raw images to be acquired is decided based on the required accuracy of the scan data.

2.5.1.2 Space Encoding

This approach involves acquiring successively projected binary patterns on the scan object. The number of patterns projected onto the scan object explicitly denotes the number of bits used in the codification. The bright regions in the pattern are assigned the logic level '1' and the dark regions are

assigned a level of ’0’. The projected patterns are assigned with different weights and thus the pixels in the images acquired associate to a unique binary code. For every shutter period of the CCD, a new pattern is projected onto the scan object. Yu et al. [52] demonstrated the use of space encoding method and polygonal mirror in the laser scanning device and Hattori et.al [53] presented a new approach using pattern shifting method. The method was tested with the objective of improving accuracy at a cost of losing acquisition speed.

2.5.1.3 Smart Sensors

For the scanning systems with a rotating mirror setup, accurate position sensors are needed to effectively control the hardware for best scan results. The rotating mirror’s motor was driven by the position controllers based on the inputs by the external rotation sensor. This complex hardware was simplified by replacing the external rotation sensor with a timer. Araki et al.[73] proposed a new method for measuring the time at which the slit image projects onto a photosensitive cell of a specifically designed discrete array. Each of the photosensitive cells has a time register associated and is incremented till the image of the laser slit illuminates its corresponding photosensitive cell. Two optical switches and a simple threshold circuit were used to trigger the start/stop process and to detect laser stripe image respectively. After a complete scan, the registered array was configured to form a bit-shift register.

Chapter 3
System Description

3.1 Scanner criteria

As mentioned previously, designing and constructing a prototype of a 3D foot scanner within a budget of CAD 7,500 was the primary objective of this research. Along with the primary objective of deploying a low cost 3D foot scanner, it was also necessary to have an output with a reasonable accuracy level and generate an open source design in the construction of the system's hardware and software components. This would enable the scanner to achieve the secondary objectives, which include sizing, feature detection and texture mapping. The following chapter describes the operations of a 3D Foot scanner that produces a three dimensional point cloud representing a person's foot. Furthermore, the 3D data points in X, Y, Z world coordinate space are used to reconstruct a CAD model.

The approximate budget for the development and construction of this 3D scanner was $ 7,500 (Canadian dollars), and compared to the professional industrial 3D foot scanners in the range of $25,000 to $75,000. It is evident from the results that the scanner was able to generate results close to the targeted accuracy level of less than 1 cm. Less computational process and simple construction make the scanner more advantageous when compared to other 3D foot scanners that are on the market.

3.2 Overall constructional setup

This section covers a brief introduction to the mechanical and electrical design of the 3D foot scanner. The mechanical design of the scanner was made by Besliu [2] and the electrical design was carried out by Jake Neilson, University of Waterloo.

3.2.1 Scanner criteria

Since the scanner was developed in collaboration with industrial sponsors, basic requirements, criteria and specifications were considered as the baseline of work and thought process throughout the hardware and software development. Some of these major criteria are discussed in this section.

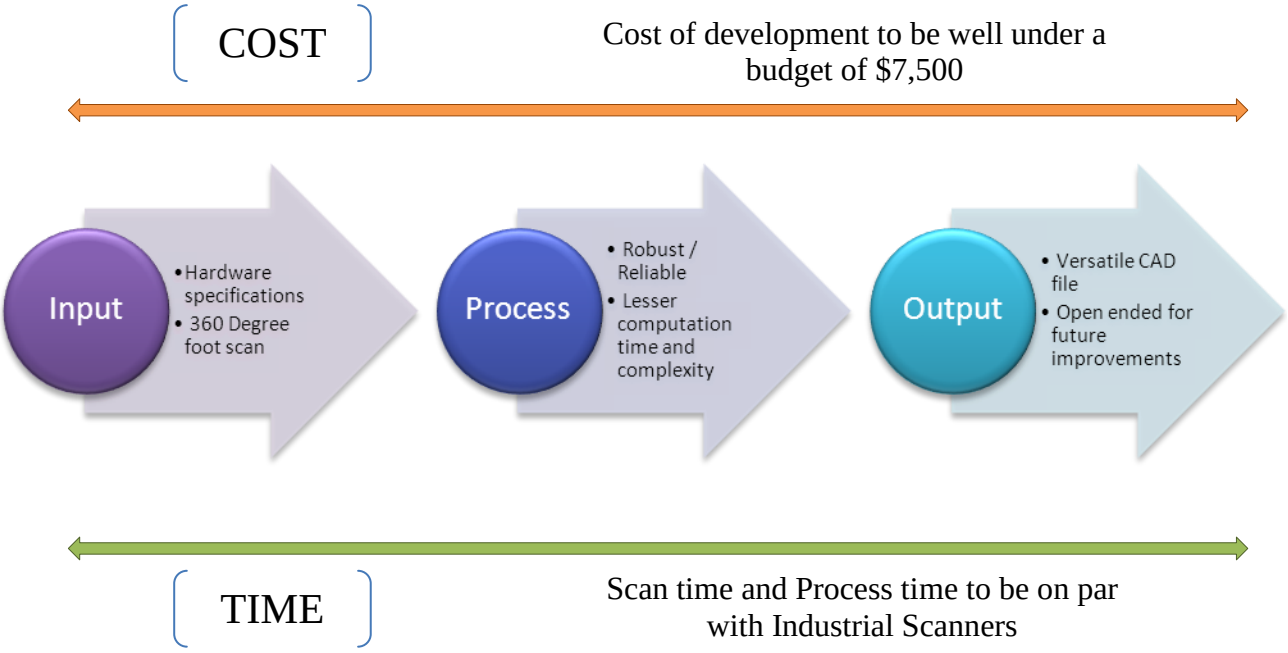

Figure 3-1 3D Foot scanner criteria

3.3 Hardware setup

3.3.1 Overall Setup

Laser- Camera range sensor setup of the scanner was designed and constructed based on the criteria discussed in the previous section. The design ensured the required scan volume of 5.5 (140 mm) inches in width, 4.5 inches (114 mm) in height and 15 inches (380mm) in depth.

In order to establish a 360 degree scan of the foot and to have a simple scanner construction/assembly, use of multiple cameras was preferred instead of choosing a rotational mirror setup or other methods that were mentioned earlier in Chapter 2. A CAD model of the developed prototype is shown in Figure 3-2 and photo views are shown in Figure 3-3 and Figure 3-4.

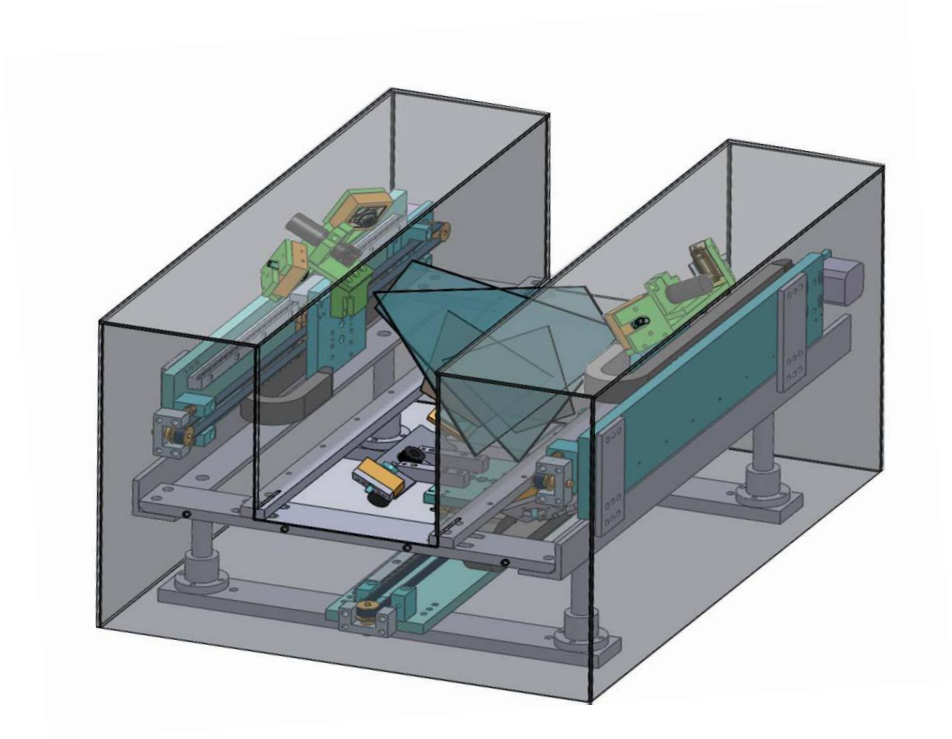

Figure 3-2 CAD model of the 3D Foot scanner with conceptual laser plane

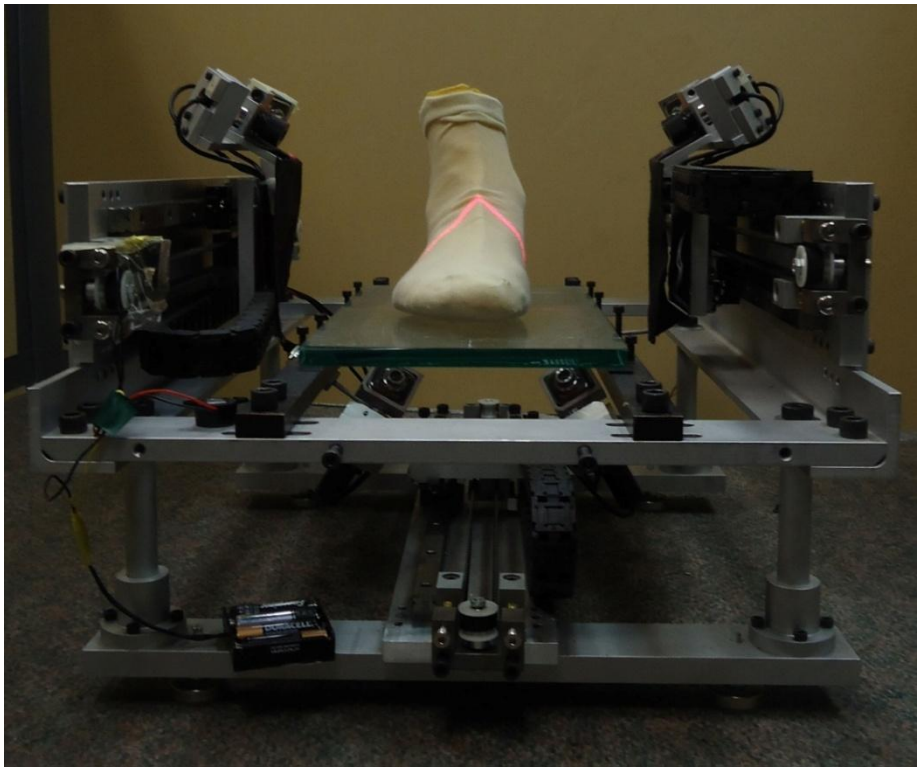

Figure 3-3 3D Foot scanner - Working prototype

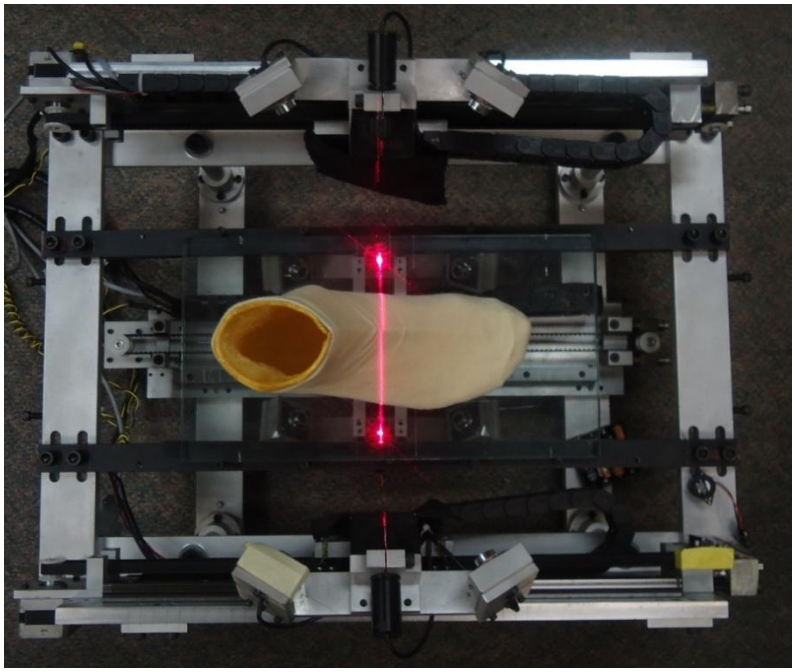

Figure 3-4 Top view of the 3D Foot scanner

3.3.2 Range-Sensor Platforms

Considering the field of view of the camera and camera parameters, the scanner setup was finalized to have 3 laser-camera range sensor heads to view the upper-left foot, upper-right foot and plantar surfaces of the foot. Each of the range sensor head that scan the upper-left region and upper-right region of the foot consists of two cameras and a laser, positioned with known geometry. The range sensor set up for the plantar surface scan consists of 4 cameras and 2 lasers. Figure 3-5 illustrates the three laser range-sensor heads in the scanner. More detailed construction is shown in Figure 3-6.

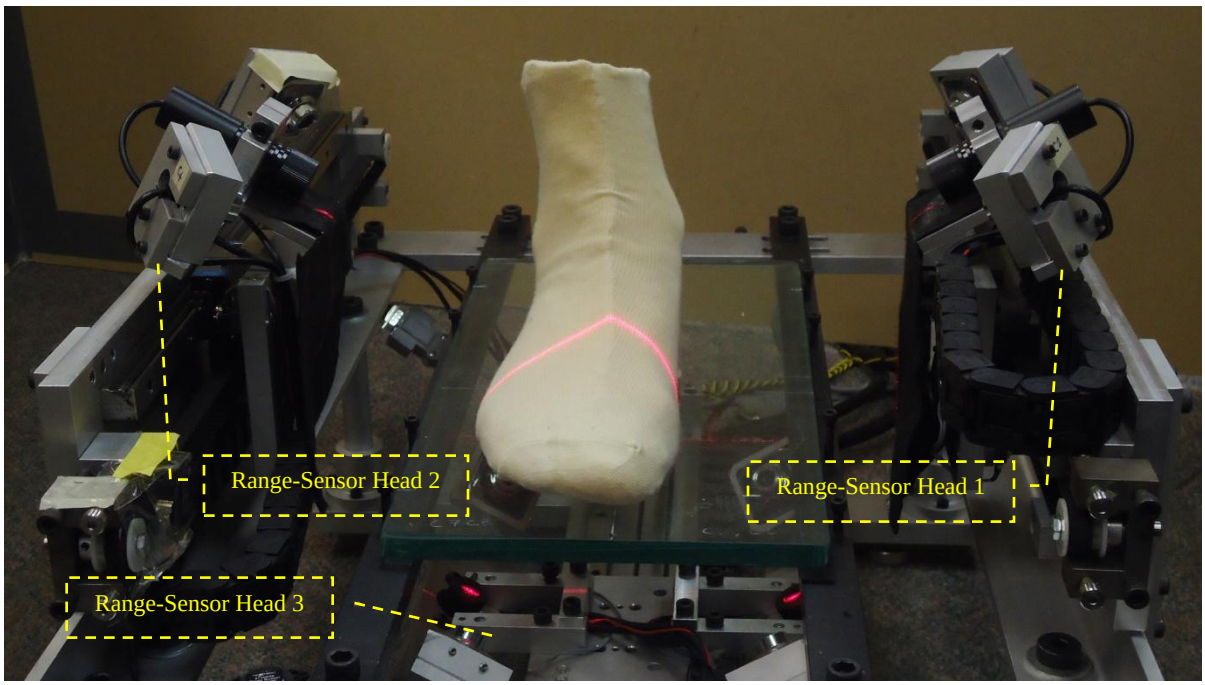

Figure 3-5 Range sensor head - Overview

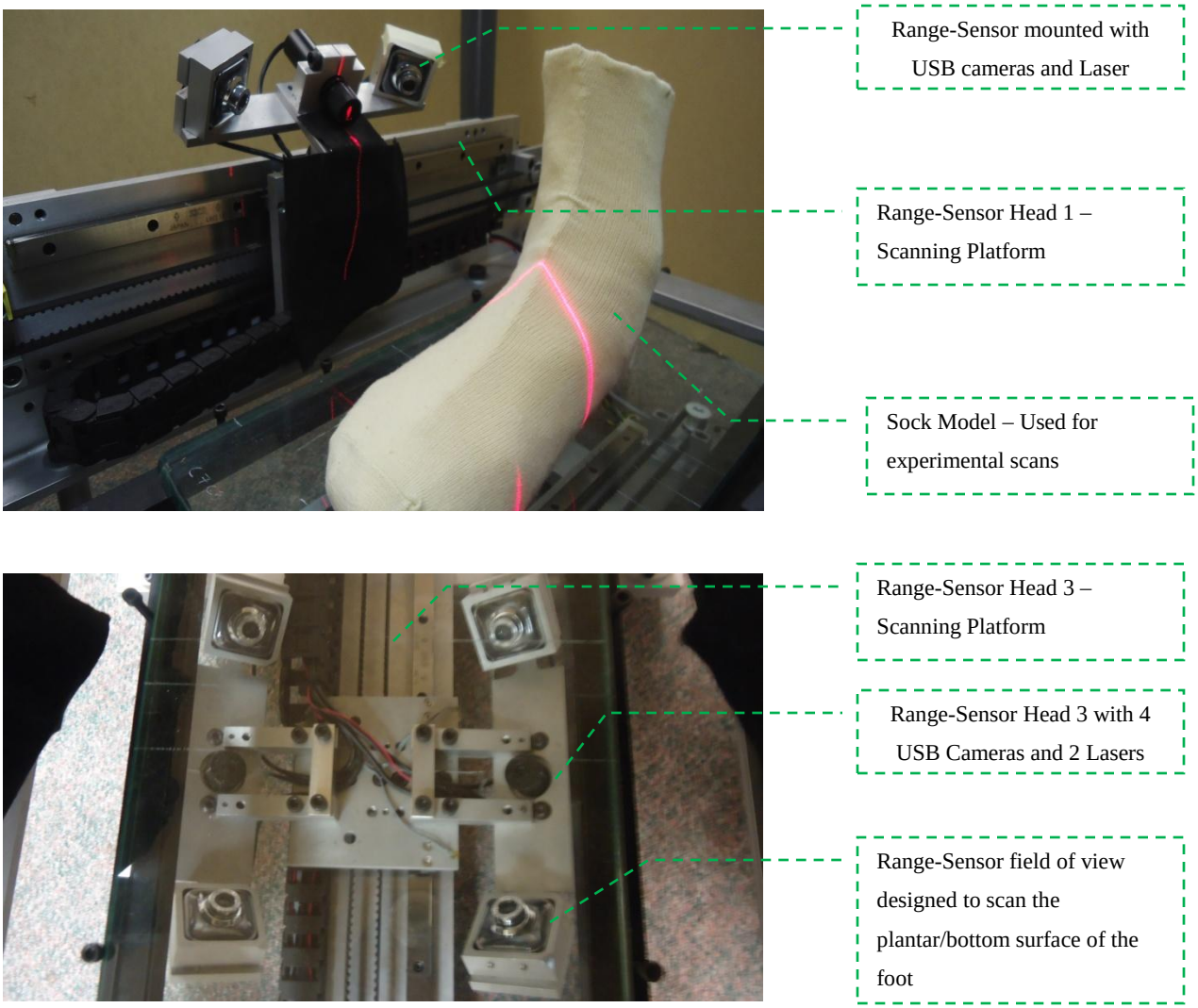

Figure 3-6 From top to bottom (1) Range sensor head - Side platform (2) Range sensor head - Bottom platform

All the range sensor heads utilize a compact 1.3MP PC USB 2.0 webcam and high powered (50mW) red lasers. The chosen cameras fit well with the prototype design in terms of cost, resolution and size constraints. Moreover, the camera also has an adjustable focal length which permits close range measurements of 3 inches (76mm). The range sensor head was positioned such that the depth of field is 3.5 inches (89mm). It can be noted from the figure that the cameras in the range sensor head are

tilted at 42 degrees to the laser light plane. The lasers have a fan angle of 80 degrees and this is sufficient to trace the whole foot.

A brief description of the functionalities of each range sensor head is described in the Table 3-1.

Table 3-1 Functional roles of the range sensor heads

Range-Sensor Head	Description	Functionality
1	2 USB Cameras and a Laser	Scan data of the upper-left regions on foot
2	2 USB Cameras and a Laser	Scan data of the upper-right regions on foot
3	4 USB Cameras and 2 Lasers	Scan data the plantar/bottom region of the foot

3.3.3 Motors and Drives

The range-sensor head's motion is actuated with stepper motors. The stepper motor is driven by a custom drive circuit with logic chips and solid state relays. The speed control is achieved by increasing or decreasing the step sequence of the drive circuitry. The hardware also has micro switches mounted on all of the range-sensor heads, which are triggered at the end of the motion. This ensures a closed loop control and helps to avoid hard stops or missing steps in the motion.

The interface between the computer, stepper motors, switches and the hand held controller was programmed within the microcontroller. The microcontroller and the logic circuitry are encapsulated into a control box, shown in Figure 3-7. The hand held controller (shown in Figure 3-8) was designed and fabricated to enable manual control of the range-sensor heads for device calibration, bug-fixes and for other experimental trials.

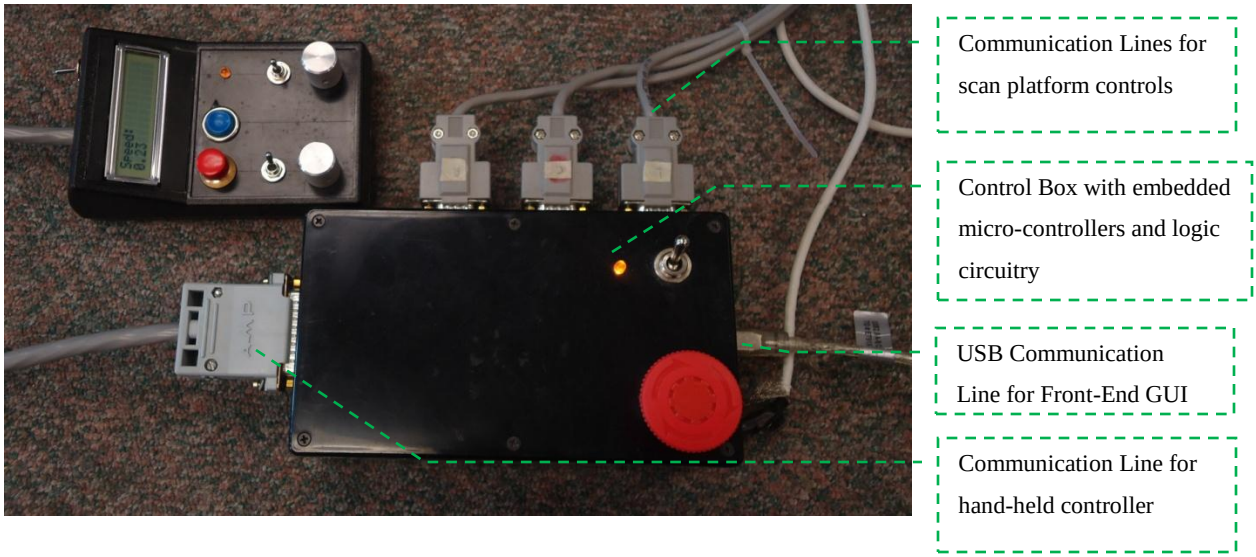

Figure 3-7 Control box

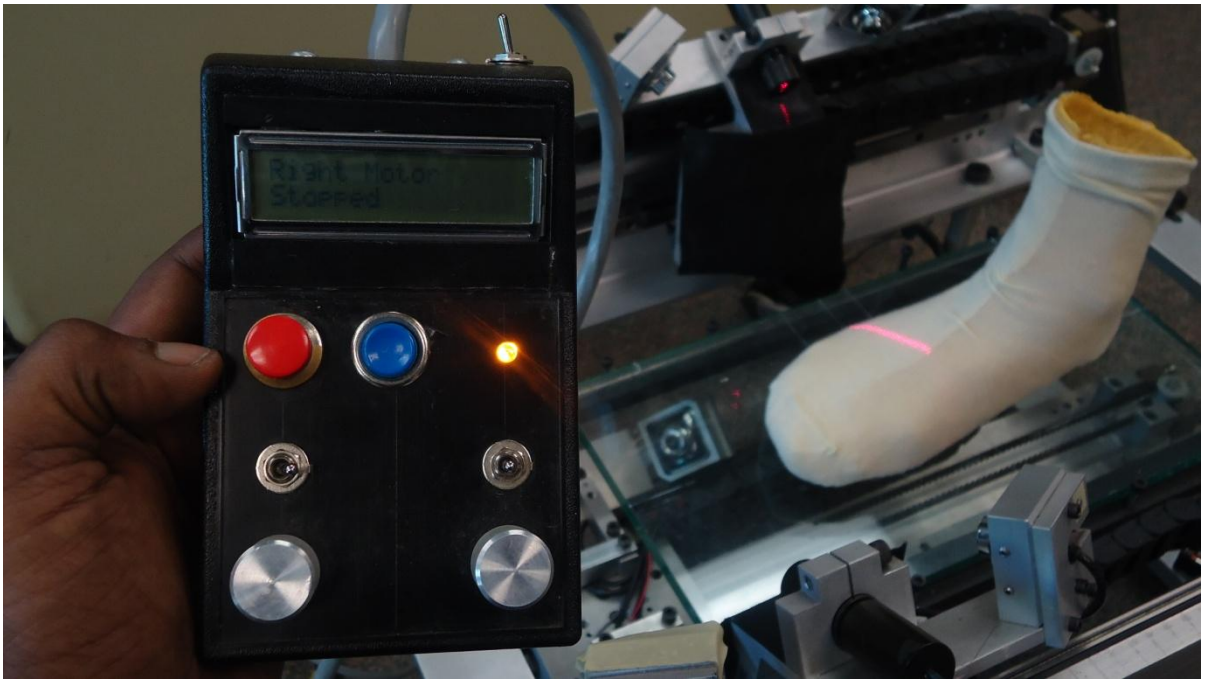

Figure 3-8 Hand-held controller

3.3.4 Front-end interface

All the hardware components mentioned in the previous sections are operated by several structured classes written in C++. The interface between the user and scanner happens through a Visual Basic Graphic User Interface. Figure 3-9 shows the GUI that runs the scanner. Subroutines scripted in Visual Basic, communicate with the embedded microcontroller in the control box for each instruction the user inputs. This concludes the overview of the electro-mechanical setup of the scanner. Subsequent sections discuss the primary research of this thesis on 3D Foot model reconstruction from the devised scanner.

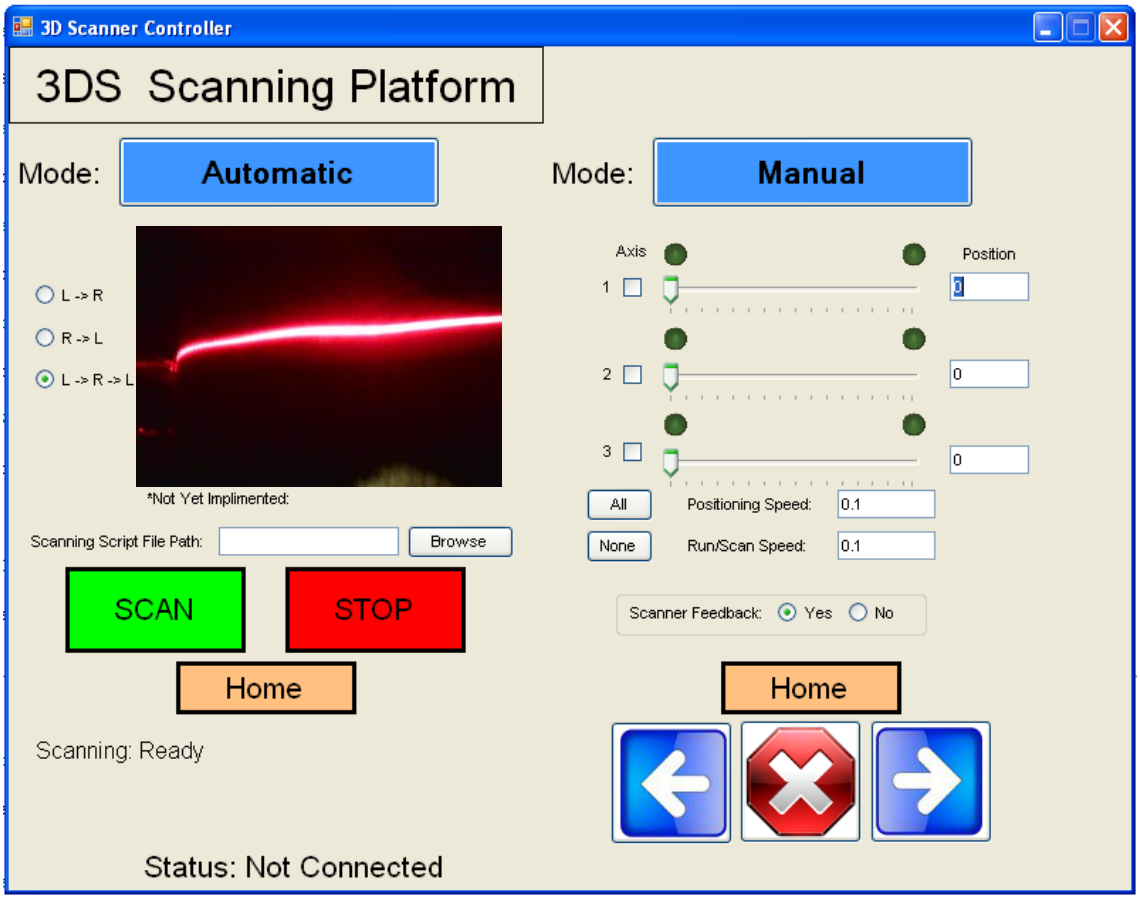

Figure 3-9 Front-end Graphic User Interface

Chapter 4
Optical Calibration of the Scanner

4.1 3D measurement process of the Foot scanner

The measurement process can be represented in four major steps: Camera calibration, Image acquisition, Digitization and 3D Reconstruction. The accuracy level and quality of these processes, determines the precision of the output measurement. Figure 4-1 illustrates the process sequence to be carried out for measuring a 3D object. The following section describes the first critical step of camera calibration. The subsequent steps are discussed in Chapter 5 of the thesis.

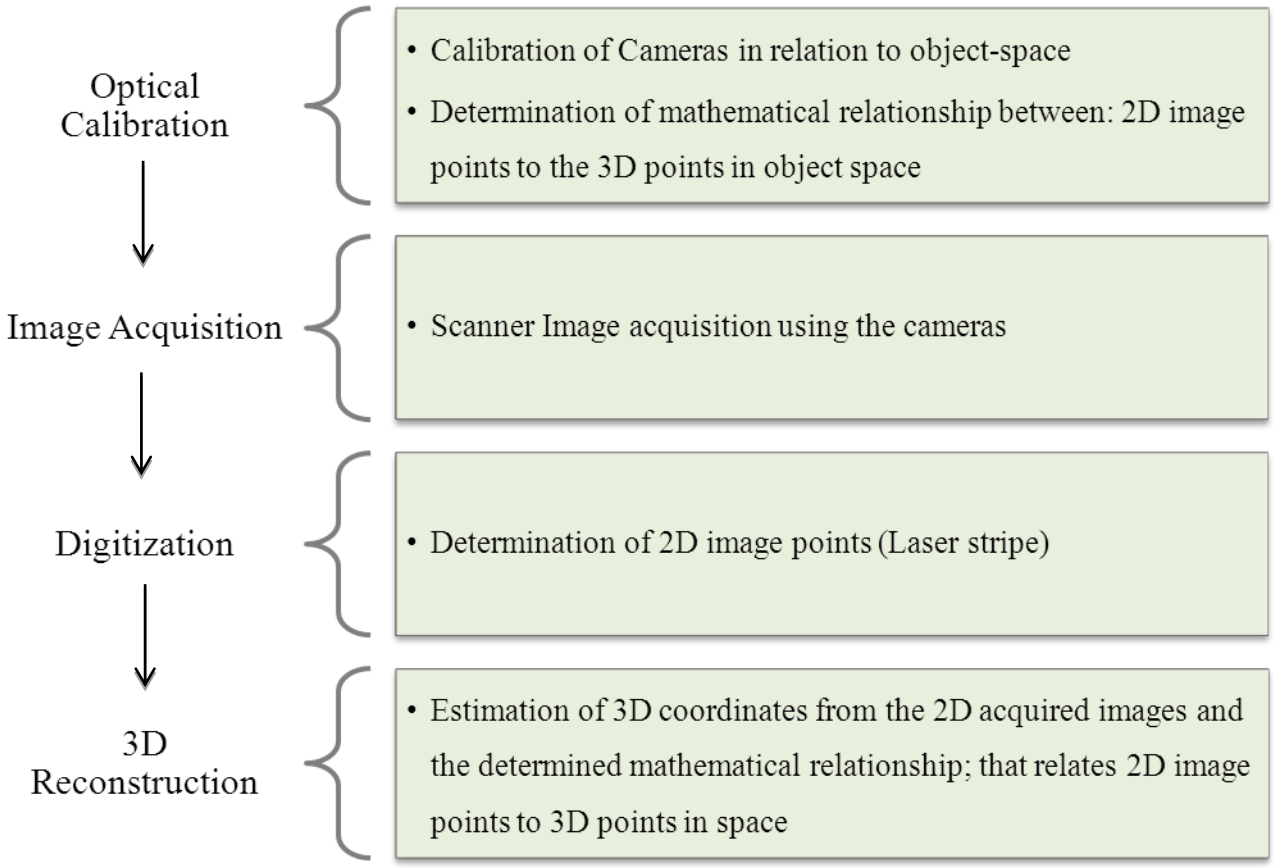

Figure 4-1 Basic steps in image-based 3D measurement

4.2 Optical Calibration

Optical calibration or camera calibration deals with determining a mathematical relationship between the 2D image points of an image to their corresponding 3D points in a space frame referenced to the camera focal plane. With the known mathematical relationship, 3D data points can be acquired from any 2D image points of the calibrated camera. As mentioned in the previous chapter, 8 cameras were used in the foot scanner. This requires calibrating all 8 cameras with high precision to yield reliable output.

As discussed in Chapter 2.4, the majority of the calibration of laser-scanner range sensor employed triangulation techniques. The triangulation technique has proven to be effective, but the complexity in computation and precise details on intrinsic and extrinsic parameters of the cameras used, makes it more difficult to apply to this scanner setup. Based on the criteria devised for the scanner, it was essential to apply a technique that yielded an accurate relationship between the input and output data of the 8 cameras both quickly and with few computations.

4.2.1 Choosing a calibration technique

Choosing a calibration technique for the scanner was carried out purely based on the cameras used in the device. For example, calibration method and complexity differs from cameras with known optical parameters to cameras with unknown optical parameters. This study was carried out in two cases; Calibration with known parameters and calibration with unknown camera parameters.

4.2.1.1 Known parameters

For cameras with known intrinsic, extrinsic parameters and setup parameters, 3D coordinates (X,Y,Z) can be determined from geometric equations relating to the image coordinates (i,j) and (X,Y,Z) [67]. Intrinsic parameters of these cameras are known prior to the usage. Typically, these cameras are

referred to as ‘metric cameras’ whose parameters are estimated and well defined by the manufacturer. Extrinsic parameters and setup parameters like distance and angles between cameras/laser are computed and calibrated accordingly.

4.2.1.1.1 Drawbacks

- Metric cameras are expensive.
- Highly sensitive to setup parameters. Cameras using this method require extremely accurate alignment of cameras in terms of angles and distances.

4.2.1.2 Unknown Parameters

These cameras are also referred to as ‘non-metric’ cameras. The camera parameters and setup details are unknown and are determined by calibration routine rather than physical measurements. The camera’s internal and setup parameters are usually determined implicitly or explicitly as mentioned in section 2.4.2 of this thesis.

4.2.1.2.1 Major advantages

- Measurement of camera angles, distances and other geometries are not required.
- Less-expensive off-the shelf cameras can be used.
- Easy handling and wider scope of applications.

Except for the setup parameters, intrinsic and extrinsic parameters of the 8 USB web cameras used in the foot scanner were unknown. Moreover, the prototype was subjected to continuous alterations in hardware as a part the research. Any disturbances in the optical setup after calibration would alter the results and would require recalibration. This would furthermore increase the complexity of the

scanner in its real world application. Hence, a robust and quick calibration method was the need. This motivated the design and use of a reference object based calibration method.

As mentioned earlier in section 2.4.1, a reference object based calibration method involves the optical system observing an object of well-known geometry in world space and the corresponding relationship is computed between the geometry of the object in the image coordinate system to that of the world coordinate system.

4.3 Fast and Robust calibration technique

The mathematical relationship that relates the 2D image points to the 3D data points are estimated by Multivariate polynomial regression. Figure 4-2 shows the basic transformation of 2D image data into 3D world space data. The following section discusses the mathematical approach for establishing the relationship by the multivariate polynomial regression method in detail.

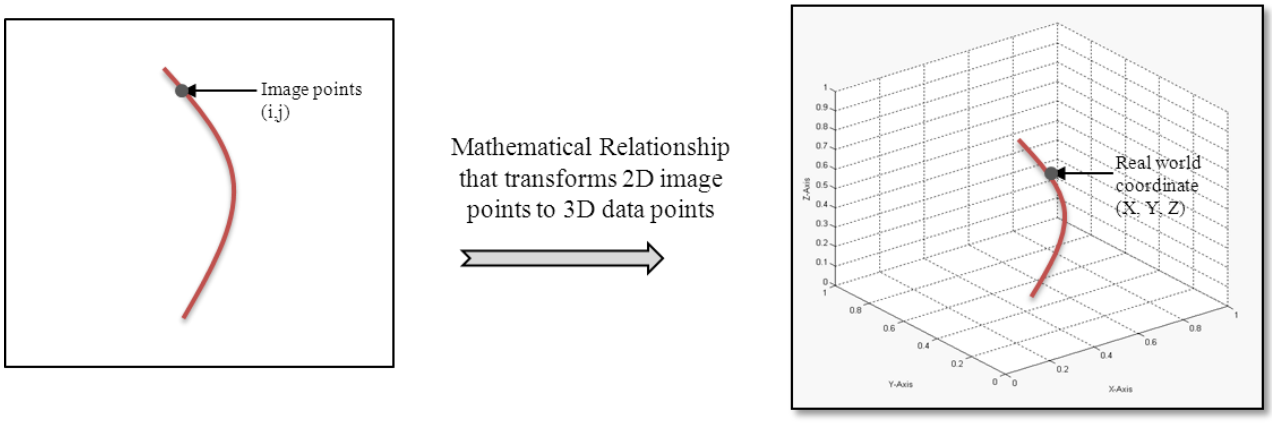

Figure 4-2 Transformation of 2D image data points to world space

4.3.1 Depth Mapping - Multivariate Regression

The entire process of calibration revolves around the mapping of image points (i, j) to real-world coordinates (X, Y, Z). The mapping of these variables is achieved by the polynomial regression method. The method is a form of linear regression that permits the output variable to be predicted by decomposing the input variable into an n^{th} order polynomial. This method is widely applied in fitting nonlinear data into a least squares linear regression model.

Generally the regression model has the form:

$$R = \alpha_0 + \alpha_1 p + \alpha_2 p^2 + \alpha_3 p^3 + ...\alpha_k p^k \tag{4.1}$$

Where,

α_0, α_1, α_2, α_3, .. α_k - Polynomial coefficients

R - Output variable

p - Input variable

As the successive powers of the ' p ' are added to the equation, the best fit line changes shape. As such, it results in changes in input-output relationship as well.

For example,

$R = \alpha_0 + \alpha_1 p$ .. (Produces a straight line; Figure 4-3 (a))

$R = \alpha_0 + \alpha_1 p + \alpha_2 p^2$ .. (Quadratic: Produces a parabola; Figure 4-3 (b))

$R = \alpha_0 + \alpha_1 p + \alpha_2 p^2 + \alpha_3 p^3$ ..(Cubic: Produces 's' shaped curve; Figure 4-3 (c))

Figure 4-3 illustrates the variation of the relationship with the degree of the polynomial equation.

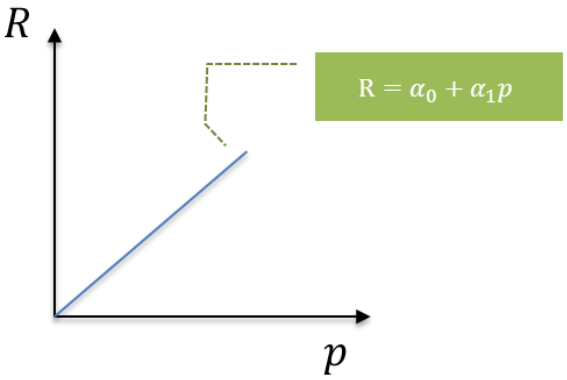

Figure 4-3 (a): First degree polynomial

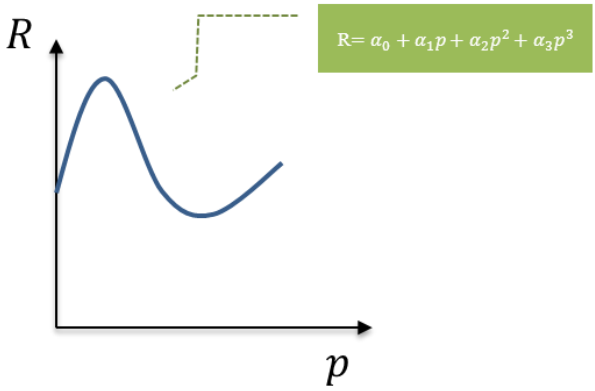

Figure 4-3 (c): Third degree polynomial

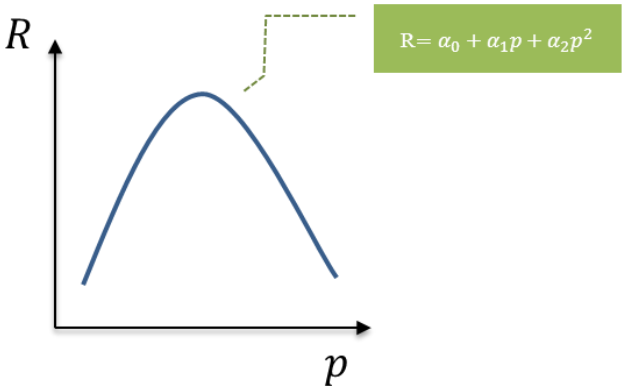

Figure 4-3 (b): Second degree polynomial

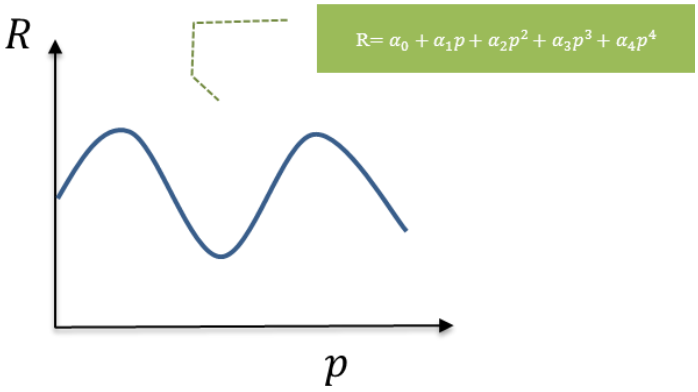

Figure 4-3 (d): Fourth degree polynomial (permits more kinks and knots)

Figure 4-3 Polynomial curves of various orders

For mapping between the image coordinates and the real world coordinates, a quadratic polynomial relationship is preferred as the foot profile data are of this type. The above discussed polynomial yields the relationship for one input and one output. But, for calibrating 2D images into 3D real world

coordinates, where ‘i’ and ‘j’ are to be mapped to their corresponding ‘Y’ and ‘Z’ (‘X’ is fixed as the range-sensor calibration is done in the YZ plane).

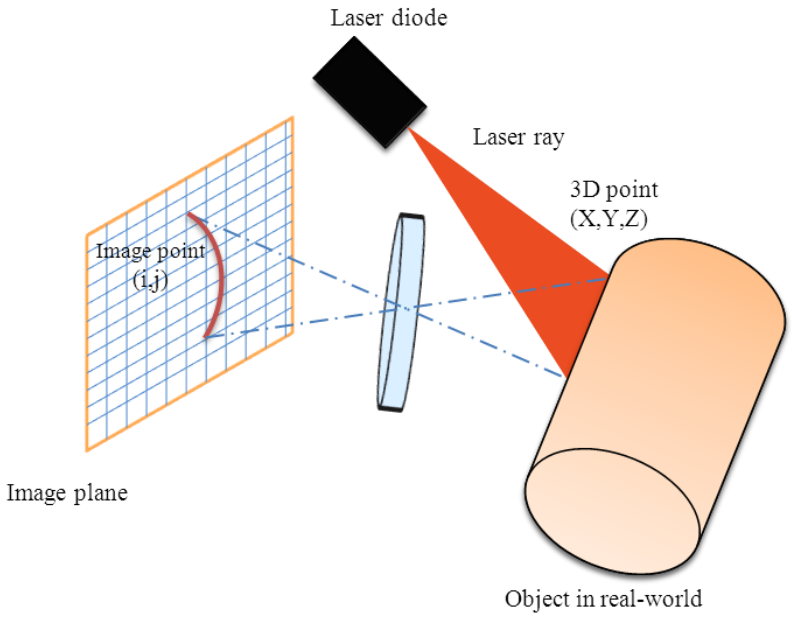

Figure 4-4 Conceptual diagram of laser ray over an object and its view in image plane

For this requirement, equation 4.2 shows an example of how the relationship is established based on two inputs (p, q) and the output (R).

A second order polynomial function of two variables generally has the form,

$$R = f(p,q) = \alpha_1 + \alpha_2 p + \alpha_3 q + \alpha_4 p^2 + \alpha_5 pq + \alpha_6 q^2 \quad (4.2)$$

Where,

α_1, $\alpha_2, \alpha_3, \alpha_4, \alpha_5, \alpha_6$ - Polynomial coefficients

R - Output variable

p, q - Input variables

Extending equation 4.2 to 'n' data points $\{(p_k, q_k, R)\}_{k=1}^{n}$, we obtain a model with 'n' equations for six unknowns $\{\alpha_l\}_{l=1}^{6}$

$$R_k = \alpha_1 + \alpha_2 p_k + \alpha_3 q_k + \alpha_4 {p_k}^2 + \alpha_5 p_k q_k + \alpha_6 {q_k}^2 \quad (4.3)$$

Where, k= 1… n

Equation 4.3 is represented in matrix form as:

$$\begin{pmatrix} R_1 \\ R_2 \\ R_3 \\ . \\ . \\ R_n \end{pmatrix} = \begin{pmatrix} 1 & p_1 & q_1 & {p_1}^2 & p_1 q_1 & {q_1}^2 \\ 1 & p_2 & q_2 & {p_2}^2 & p_2 q_2 & {q_2}^2 \\ 1 & p_3 & q_3 & {p_3}^2 & p_3 q_3 & {q_3}^2 \\ . & . & . & . & . & . \\ . & . & . & . & . & . \\ 1 & p_n & q_n & {p_n}^2 & p_n q_n & {q_n}^2 \end{pmatrix} \begin{pmatrix} \alpha_1 \\ \alpha_2 \\ \alpha_3 \\ \alpha_4 \\ \alpha_5 \\ \alpha_6 \end{pmatrix} \quad (4.4)$$

which can be written as:

$$[R] = [M_{p,q}].[\alpha] \quad (4.5)$$

Where,

$$[R] = \begin{pmatrix} R_1 \\ R_2 \\ R_3 \\ . \\ . \\ R_n \end{pmatrix} \qquad \left[M_{p,q}\right] = \begin{pmatrix} 1 & p_1 & q_1 & p_1^{\,2} & p_1q_1 & q_1^{\,2} \\ 1 & p_2 & q_2 & p_2^{\,2} & p_2q_2 & q_2^{\,2} \\ 1 & p_3 & q_3 & p_3^{\,2} & p_3q_3 & q_3^{\,2} \\ . & . & . & . & . & . \\ . & . & . & . & . & . \\ 1 & p_n & q_n & p_n^{\,2} & p_nq_n & q_n^{\,2} \end{pmatrix} \qquad [\alpha] = \begin{pmatrix} \alpha_1 \\ \alpha_2 \\ \alpha_3 \\ \alpha_4 \\ \alpha_5 \\ \alpha_6 \end{pmatrix}$$

4.3.2 Computation

Equation 4.5 serves as the base to compute the mathematical relationship between the 2D image points (i,j) and the real world coordinates (X, Y, Z). If $[R]$ and $\left[M_{p,q}\right]$ represent the real world coordinates and the image coordinates respectively, $\left[M_{p,q}\right]$ can be computed from the image data points and with the known coefficient matrix $[\alpha]$, its corresponding $[R]$ can be computed.

The image points of the laser profile to construct $\left[M_{p,q}\right]$ are acquired through the image processing module of the software (details in Chapter 5) and the coefficient matrix $[\alpha]$ is obtained through the range sensor calibration.

The calibration is carried out in the ‘YZ’ plane with a fixed ‘X’ coordinate. Hence, the polynomial equation is extended for two variables ‘Y’ and ‘Z’. This allows computing the relationship of ‘Y’ coordinates and ‘Z’ coordinates with the 2D image points independently. The equations are constructed as follows.

Equation to map ‘Y’ coordinates with the image points (i, j):

$$\begin{pmatrix} Y_1 \\ Y_2 \\ Y_3 \\ . \\ . \\ Y_n \end{pmatrix} = \begin{pmatrix} 1 & i_1 & j_1 & i_1^2 & i_1 j_1 & j_1^2 \\ 1 & i_2 & j_2 & i_2^2 & i_2 j_2 & j_2^2 \\ 1 & i_3 & j_3 & i_3^2 & i_3 j_3 & j_3^2 \\ . & . & . & . & . & . \\ . & . & . & . & . & . \\ 1 & i_n & j_n & i_n^2 & i_n j_n & j_n^2 \end{pmatrix} \begin{pmatrix} \alpha_{y1} \\ \alpha_{y2} \\ \alpha_{y3} \\ \alpha_{y4} \\ \alpha_{y5} \\ \alpha_{y6} \end{pmatrix} \tag{4.6}$$

The equation can be re-written as,

$$\left[Y\right] = \left[\text{Pix}\right].\left[\alpha_y\right] \tag{4.7}$$

It should be noted that, the matrix $\left[\text{Pix}\right]$ is similar to $\left[M_{p,q}\right]$. The notation is changed for better understanding of computations involving image points (i,j).

Similar to equation 4.6, the equation to map ‘Z’ coordinates with the image points (i, j) can be constructed as,

$$\begin{pmatrix} Z_1 \\ Z_2 \\ Z_3 \\ . \\ . \\ Z_n \end{pmatrix} = \begin{pmatrix} 1 & i_1 & j_1 & i_1^2 & i_1 j_1 & j_1^2 \\ 1 & i_2 & j_2 & i_2^2 & i_2 j_2 & j_2^2 \\ 1 & i_3 & j_3 & i_3^2 & i_3 j_3 & j_3^2 \\ . & . & . & . & . & . \\ . & . & . & . & . & . \\ 1 & i_n & j_n & i_n^2 & i_n j_n & j_n^2 \end{pmatrix} \begin{pmatrix} \alpha_{z1} \\ \alpha_{z2} \\ \alpha_{z3} \\ \alpha_{z4} \\ \alpha_{z5} \\ \alpha_{z6} \end{pmatrix} \tag{4.8}$$

Equation 4.8 can be re-written as,

$$[Z] = [\text{Pix}].[\alpha_z] \tag{4.9}$$

With equations 4.7 and 4.9, the real world coordinates (X, Y and Z) can be computed from the image points and the coefficient vectors $[\alpha_y]$ and $[\alpha_z]$. The calibration of the range sensor is basically the process of computing the co-efficient vectors so that the image data points are mapped to the real-world data.

From equations 4.7 and 4.9, $[\alpha_y]$ and $[\alpha_z]$ can be determined in a least-squares *pseudo inverse* method:

$$[Y] = [\text{Pix}][\alpha_y]$$

Pre-multiply both sides by $[\text{Pix}^{\text{T}}]$:

$$[\text{Pix}^{\text{T}}][Y] = [\text{Pix}^{\text{T}}][\text{Pix}][\alpha_y]$$

Pre-multiply both sides by $[\text{Pix}^{\text{T}}\text{Pix}]^{-1}$:

$$[\text{Pix}^{\text{T}}\text{Pix}]^{-1}[\text{Pix}^{\text{T}}][Y] = [\text{Pix}^{\text{T}}\text{Pix}]^{-1}[\text{Pix}^{\text{T}}][\text{Pix}][\alpha_y]$$

Rearranging, the co-efficient matrix $[\alpha_y]$ is determined by,

$$\boxed{[\alpha_y] = [\text{Pix}^{\text{T}}\text{Pix}]^{-1}[\text{Pix}^{\text{T}}][Y]} \tag{4.10}$$

Similarly the co-efficient matrix $[\alpha_z]$ is determined as,

$$[\alpha_z] = \left[\mathrm{Pix}^{\mathrm{T}} \mathrm{Pix} \right]^{-1} [\mathrm{Pix}^{\mathrm{T}}][Z] \tag{4.11}$$

4.3.2.1 Estimation of the Coefficient Matrix

Estimation of the co-efficient matrix results in a model that relates the image points to the 3D real world data. To compute the co-efficient matrix, reference object based calibration needs to be carried out.

A 3D object (as shown in Figure 4-5) of well-known geometry and high precision (+-0.001mm) was manufactured for calibrating the cameras in the foot scanner. Control points with precisely known real-world coordinates (X, Y, and Z) are chosen and marked on the 3D object. The object was positioned in the scan volume of the scanner such that, the laser ray traces over the chosen control points (Points on the reference object, that defines the relationship between the input and output parameters). It was also ensured that the object was positioned the optimum field of view of all the cameras. The setup was ensured to have no optical or physical disturbances, to minimize errors during the process.

Figure 4-5 Reference object used for calibration of 8 cameras

Once properly setup, images are captured from all 8 cameras. The image points (i, j) of the control points were identified and recorded from the captured images. It should be noted that, the precision of identifying the image points has a significant effect on the accuracy of calibration. Algorithms for image processing techniques like edge/blob detection; image segmentation and pattern recognition can be of much help in getting to sub-pixel level accuracy of detecting the control points. Table 4-1 shows a typical calibration chart for a single camera.

The known real-world coordinates of the control points (in Y and Z) constitute $[Y]$, $[Z]$ matrix and the corresponding image coordinates are constructed as $[\mathrm{Pix}]$ matrix. With the known matrices, co-efficient matrix is computed by the equations 4.10 and 4.11.

Table 4-1 Calibration chart- Depth mapping through a reference object of known geometry

	Real World Coordinates			Image Coordinates	
Control Point Number	X	Y	Z	Column (i)	Row (j)
P1	X	Y_1	Z_1	i_1	j_1
P2		Y_2	Z_2	i_2	j_2
P3		Y_3	Z_3	i_3	j_3
P4		Y_4	Z_4	i_4	j_4
P5		Y_5	Z_5	i_5	j_5
P6		Y_6	Z_6	i_6	j_6

4.4 Experiments and Trials performed

The reference object shown in Figure 4-4 was used to calibrate the range sensor heads of the scanner. This involves a process of mapping of image points from all the 8 cameras to their corresponding real world coordinates.

The reference object was placed on the scan volume of the scanner and the laser stripe was positioned over the chosen control points on the object (as shown in Figure 4-6). Following this, images representing the profile of the laser over the object were captured from all the cameras.

With the Matlab image processing toolbox, the pixel information about all the control points in terms of columns and rows (i, j) was identified and recorded in the calibration chart. Table 4-2 shows the calibration input data sets.

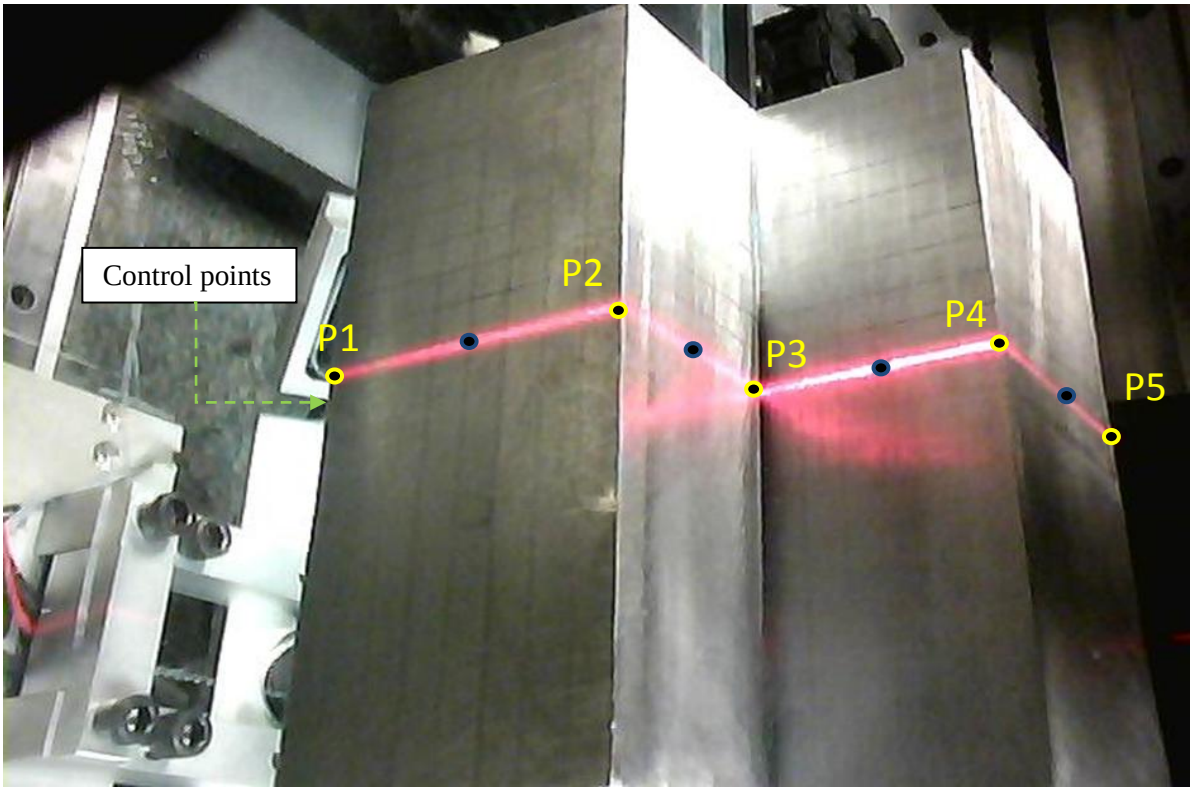

Figure 4-6 Calibration of camera 1 – Upper-left range sensor head

Table 4-2 Calibration chart of camera 1

Control Point Number	Real World Coordinates			Image Coordinates	
	X	Y	Z	Column (i)	Row (j)
P1	0	5	3	159	221
P2		5	7	318	170
P3		2	7	397	225
P4		2	10	530	192
P5		-2	10	591	255

Based on the tabulated data, the matrices $[Y]$, $[Z]$ and $[\mathrm{Pix}]$ are constructed as shown below.

Real world data (column vectors):

$$[Y]=\begin{bmatrix}5\\5\\2\\2\\-2\end{bmatrix} \qquad [Z]=\begin{bmatrix}3\\7\\7\\10\\10\end{bmatrix}$$

Image points matrix:

$$[\mathrm{Pix}]=\begin{bmatrix}1 & 159 & 221 & 159^2 & (159*221) & 221^2\\ 1 & 318 & 170 & 318^2 & (318*170) & 170^2\\ 1 & 397 & 225 & 397^2 & (397*225) & 225^2\\ 1 & 530 & 192 & 530^2 & (530*192) & 192^2\\ 1 & 591 & 255 & 591^2 & (591*255) & 255^2\end{bmatrix}$$

The above matrices are substituted in equation 4.10 and 4.11 to determine the coefficients. The result is shown in Table 4-3.

Table 4-3 Computed coefficients for 'Y' and 'Z'- Camera 1

Camera 1					
Real World		Image Point		Resultant Coefficients	
Y	Z	i	j	$[\alpha_y]$	$[\alpha_z]$
5	3	159	221	0.00000	0.00000
5	7	318	170	-0.02223	-0.00871
2	7	397	225	0.13790	0.08232
2	10	530	192	0.00000	0.00000
-2	10	591	255	0.00004	0.00011
				-0.00048	-0.00036

With the computed coefficients, the mathematical model that maps the image points of camera 1 to the world space can be formulated by substituting the determined coefficient values in the equations 4.7 and 4.9.

$$[Y] = [\text{Pix}] \begin{bmatrix} 0 \\ -0.02223 \\ 0.13790 \\ 0 \\ 0.00004 \\ -0.00048 \end{bmatrix} \tag{4.12}$$

$$[Z] = [\text{Pix}] \begin{bmatrix} 0 \\ -0.00871 \\ 0.08232 \\ 0 \\ 0.00011 \\ -0.00036 \end{bmatrix} \tag{4.13}$$

With the equations 4.12 and 4.13, any known image points of camera 1 can be mapped to real world data. Figure 4-7 presents the 3D data points of the 2D image (calibration object) computed based on the discussed mathematical model.

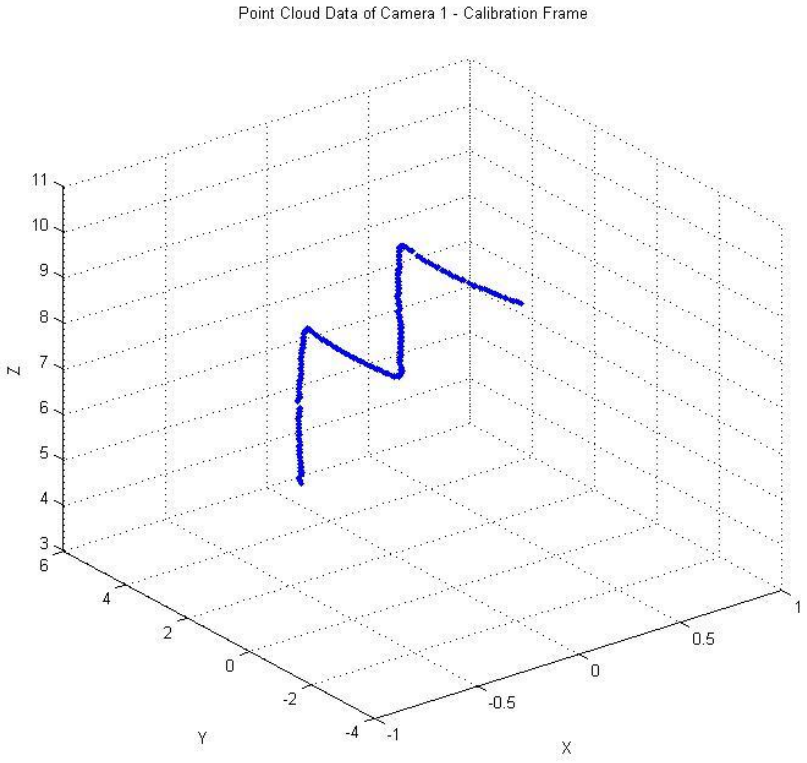

Figure 4-7 Point cloud data acquired from the calibration frame of camera 1 – 411 points

The coefficient of determination, R^2 was computed for analyzing the goodness of the equations 4.12 and 4.13. R^2 value ranges between 0 and 1; value closer to 1 indicates that the equation fits the data well. The computations are explained in Appendix A and it was found that 92.17 % of the total variance of 'Y' values and 100% of the total variance of 'Z' values are explained by variations in the input data (i,j).

The calibration chart is extended for the remaining 7 cameras and is presented in Appendix B. The data collected was loaded into the Matlab environment for computing the co-efficient matrix $[\alpha_y]$ and $[\alpha_z]$ for all the cameras. The following table shows the consolidated results of the $[\alpha_y]$ and $[\alpha_z]$ for all the 8 cameras. With the computed co-efficient matrices; the captured calibration frames from 8 cameras were processed to obtain a 3D point cloud data (shown in Figure 4-8). This step is done to verify the accuracy and precision of the calibration process.

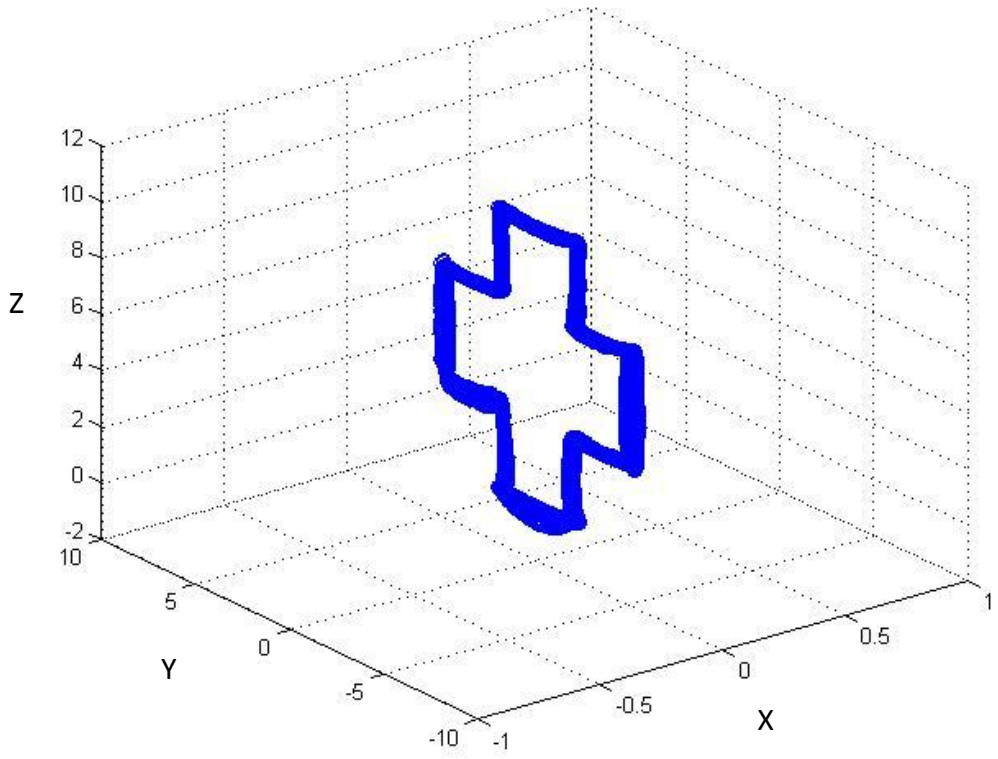

Figure 4-8 Point cloud data acquired from 8 cameras - Calibration frame

4.5 Steps after Calibration

On successful calibration of the foot scanner using the reference object, the scanner can now be used to scan and measure the human foot. A brief description of the process is illustrated in Figure 4-9.

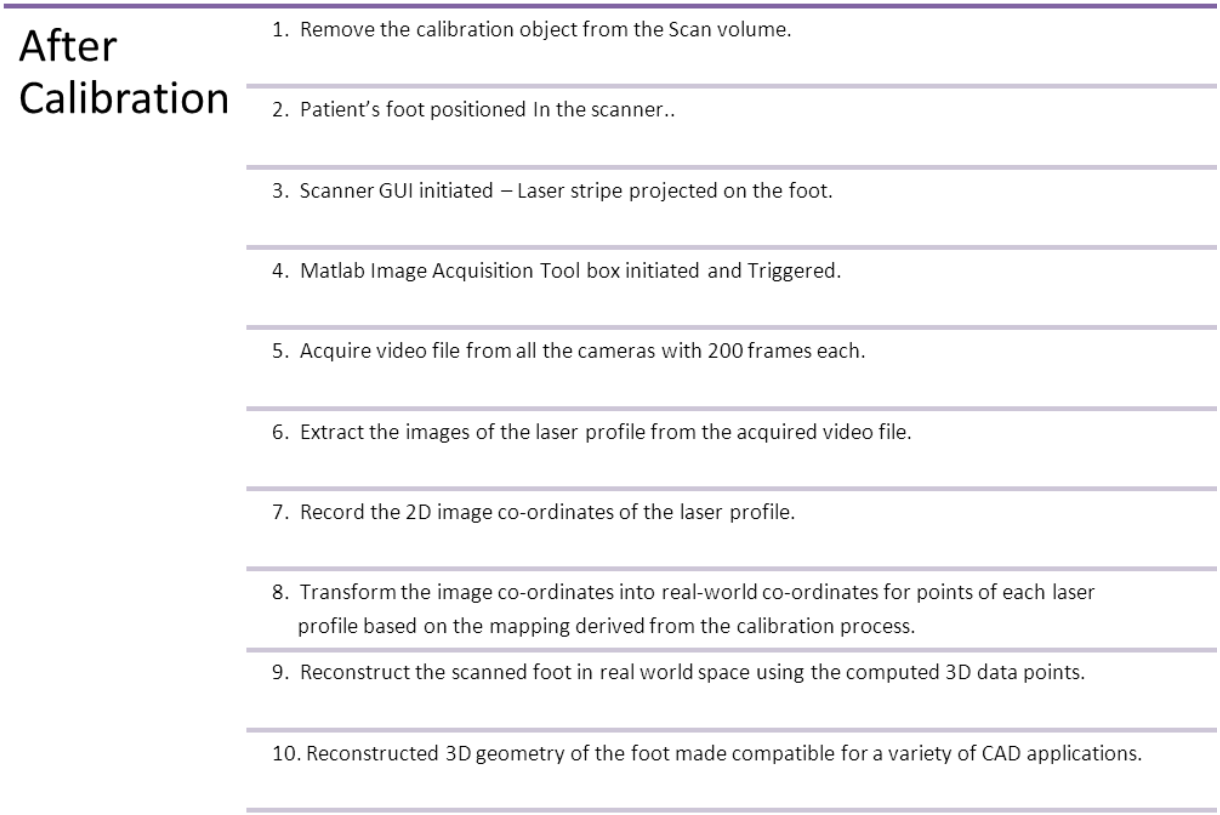

Figure 4-9 3D Foot scanning process after the calibration of scanner optical system

Chapter 5 discusses the real time data acquisition, image processing descriptions for acquiring the 2D image coordinates of the laser profile, and reconstruction from the 3D data points of the foot scan into a CAD model.

Chapter 5
Implementation and Prototype Validation

5.1 Range Image acquisition

Through calibration, a mathematical relationship between 2D image data coordinates and the 3D world space coordinates was established. The next step was to acquire 2D range image data from all the cameras in the scanning system. The following section describes the process of range image acquisition of the 3D foot scanner.

Once the subject positions their foot over the base plate of the scanner in a semi-weight bearing condition, the scanner is triggered through its GUI. The homing process takes place until all three range sensor heads are aligned axially. On successful homing, a manual trigger is initiated to capture range image data from the cameras. The Matlab Image acquisition toolbox is used to carry out the data acquisition process. Figure 5-1 shows the Matlab Image Acquisition tool working environment. Selection of cameras and defining the properties of acquisition are configured in this environment.

Avi files with 200 frames were acquired from all the cameras. Scan time for the range sensor head to cover a span of 40 cm was recorded to be 11 seconds. The number of frames was decided based on the scan area and control volume. On experimentation and trials, a collection of 200 frames was found to be suitable for covering the scan length of 40 cm. The acquisition is triggered after the successful homing operation of the range heads. The acquisition process ends after logging the set 200 frames. The file name and the logging options are configured in the acquisition tool.

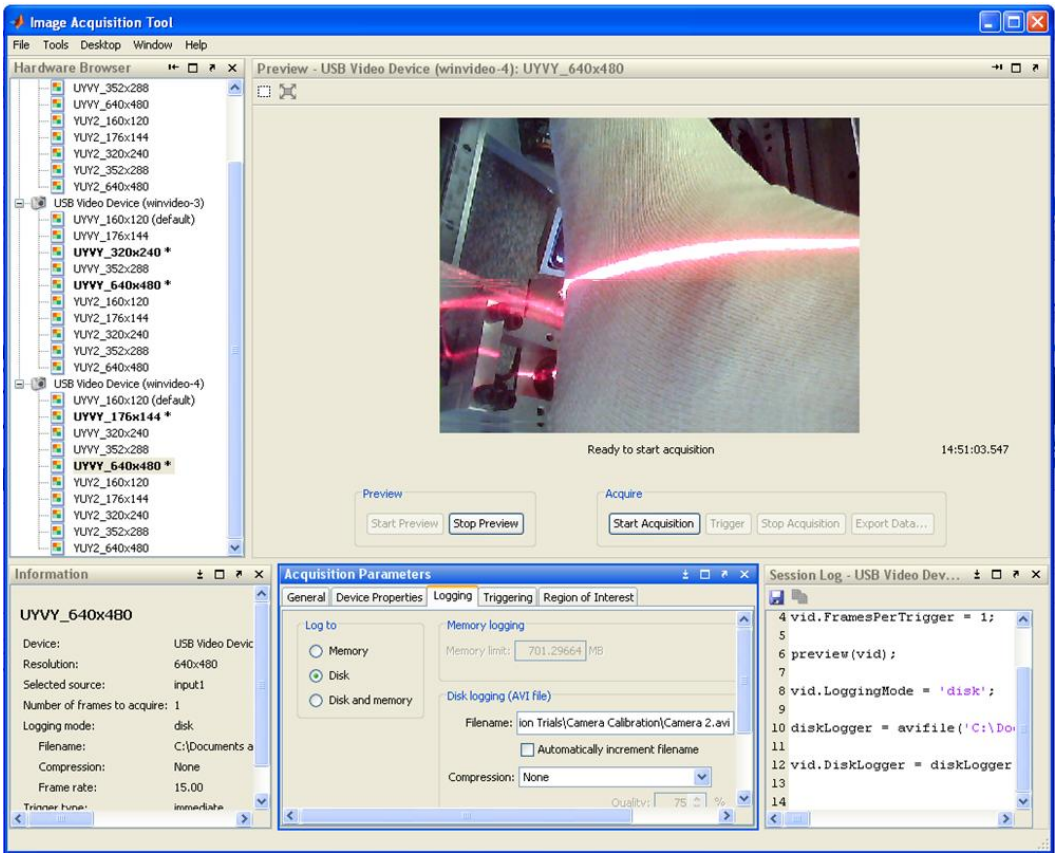

Figure 5-1 Matlab (R2010b) Image Acquisition Toolbox Environment

5.2 Image processing

Efficient extraction of the 2D range data was the primary objective of the data. Range images obtained in the earlier process are typically a series of 640x480 2D images with a laser stripe corresponding to the foot profile. Robust and simple methods of extracting the laser stripe from the range images were scripted in Matlab (R20120b) as it features a wide range of inbuilt Image processing tools.

Raw chart of the image processing module is shown in Figure 5-2. The module starts by reading the input AVI file and splitting this into frames. Following to this, frames are processed sequentially to extract 2D pixel data (i,j).

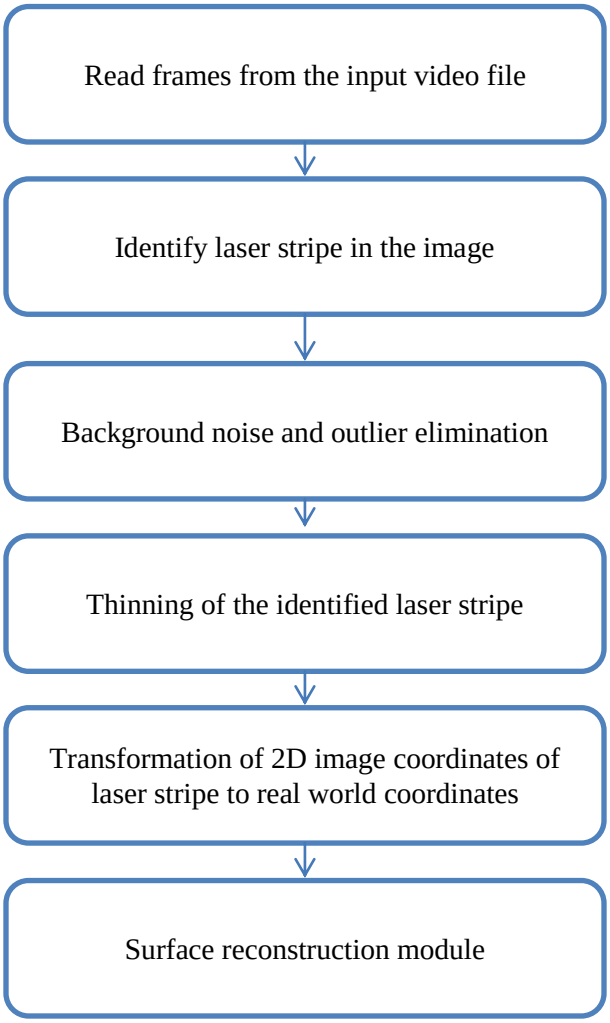

Figure 5-2 Basic overview of image processing and associated operations

The basic extraction of the laser profile from the images is through identifying the pixels corresponding to the highest intensity (255) in the red plane ie., (255,0,0). This operation is often termed 'thresholding' in image processing applications. But during the application, identification of the laser stripe could be a bit problematic, as the scanner was subject to varying ambient light conditions and the use of high-powered lasers for a short range application.

The intensity of the lasers was tuned down during dark ambient conditions and while the scanner is covered with its lid. But, for trials in ambient day light, the laser intensity was set to high so that the

cameras could capture the profile. Increasing the intensity of the laser resulted in the saturation of the laser beam over the scan object. In Figure 5-3, it can be noted that, the laser beam on top of the surface was not a pure red stripe. Rather the effect of saturation made the laser profile appear like a 3-layered band with 2 outer red layers and a white stripe through the middle. So, the preliminary step of identifying the laser profile was carried out by extracting the pixels that correspond to the 3-layered band. The thickness of the band was dependent on the material of the scan object.

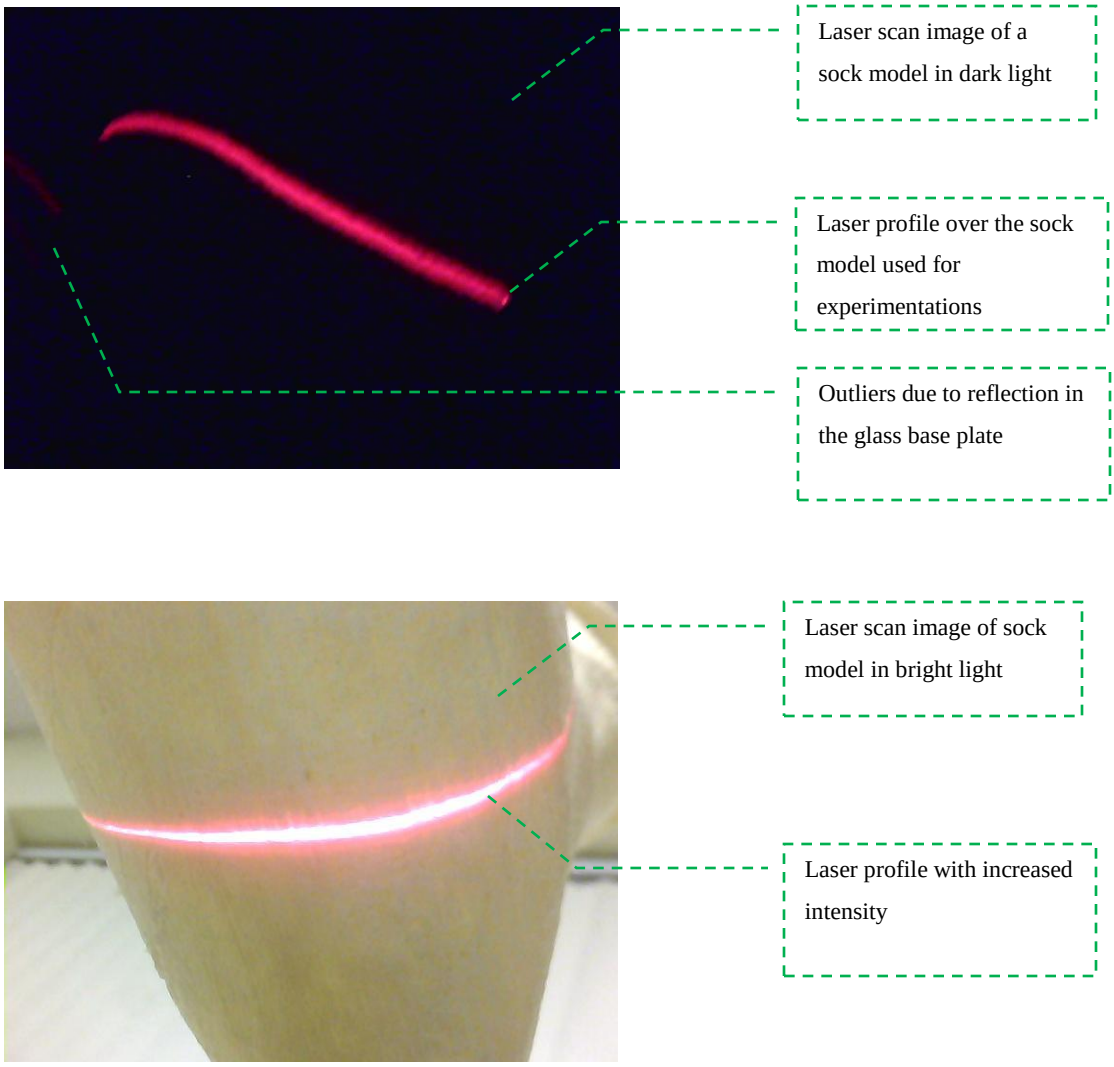

Figure 5-3 Laser profile over the sock model

Once the preliminary laser stripe is extracted, the RGB range images are converted to a binary image. The pixels corresponding to brighter regions are coded '1' and lower regions as '0'. Since, the pixels in the region of laser are naturally bright in the image; they get encoded as regions of '1'. This step also encoded the noise and outlier data pixels as '1'. At this point, a technique to isolate the continuous laser stripe from the outliers was carried out. The continuous and non-discrete laser stripe in the range image, helped to differentiate the laser stripe and the outliers.

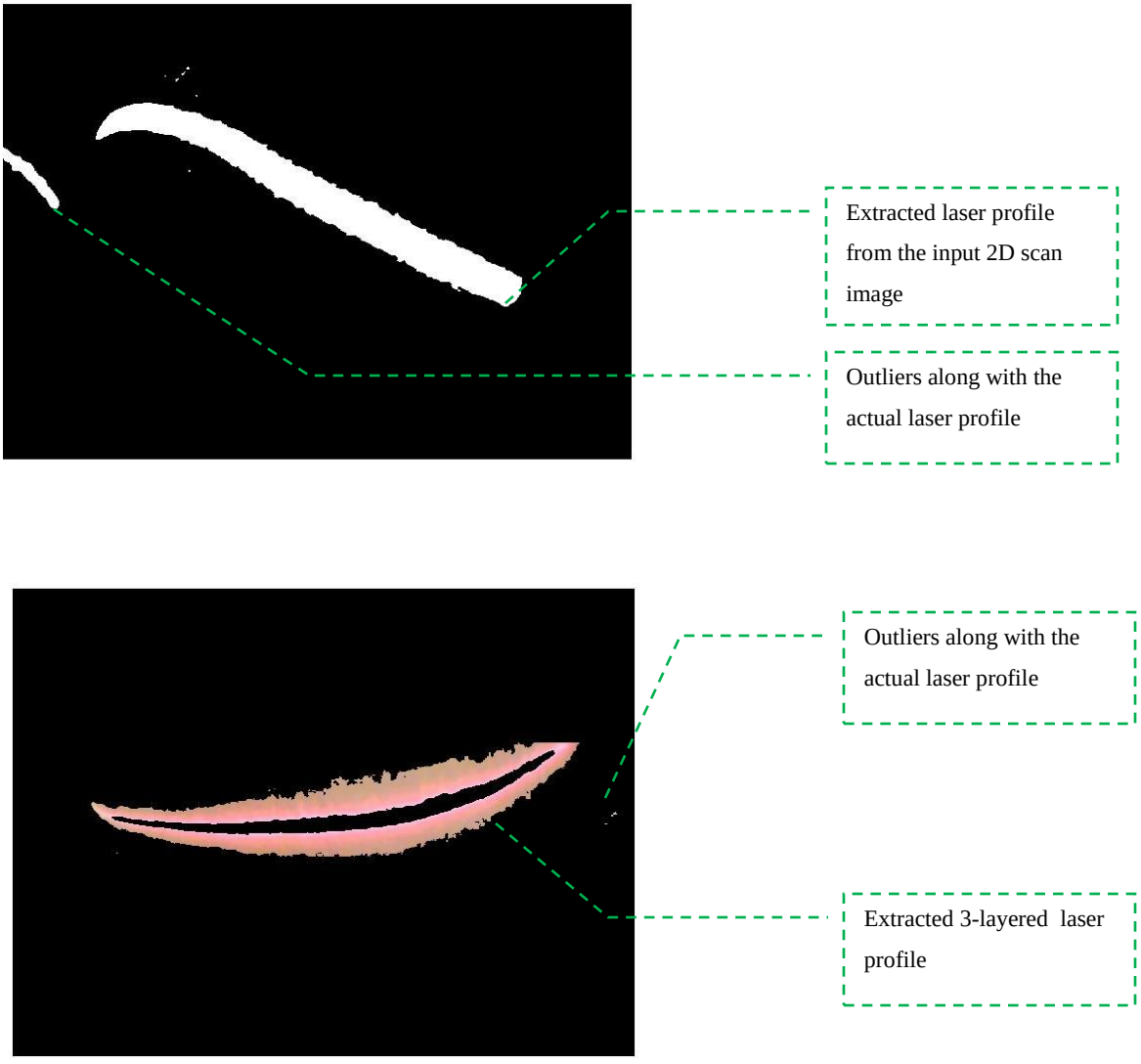

Figure 5-4 Identification of laser profile in a scan image

Following the encoding process, the encoded binary image was scanned and checked for connected pixels. The region of binary image with laser stripe had more connected pixel components than other regions. The pixels corresponding to large connectivity were then isolated to perform 'thinning/eroding'. The functions 'bwlabel' and 'bwconncomp' in Matlab were employed for this purpose.

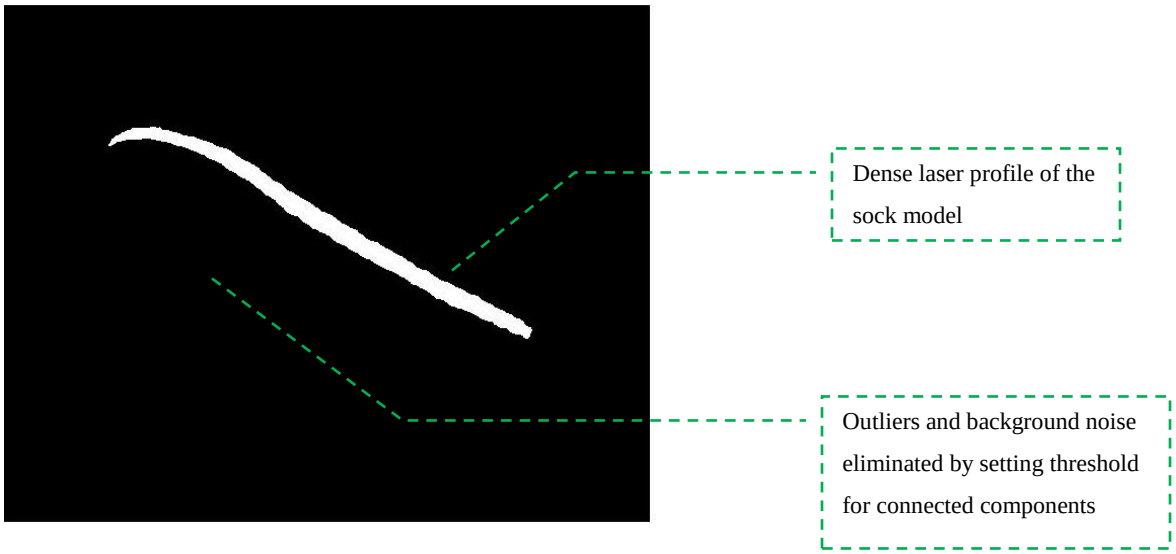

Figure 5-5 Laser profile with outliers removed

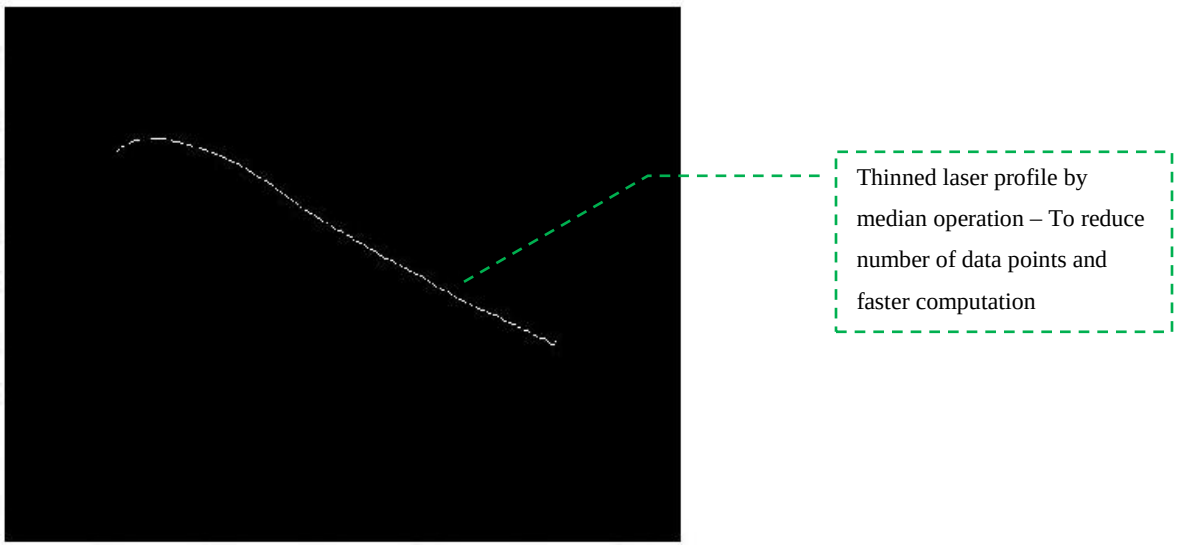

Figure 5-6 Thinned laser profile

Thinning was carried out to obtain the mid-region of the laser stripe in the range image. As discussed earlier, the saturation of laser beam over the scan object resulted in a denser pixel cloud data. The representative of the entire pixel cloud data was achieved by just extracting the median of the processed pixel cloud. This process helps in achieving a crisp and sharp pixel cloud to represent the earlier dense data.

With the above mentioned process, the laser stripe was extracted with good precision and reliability. The algorithm was successful in brighter lighting conditions (ambient) and also when the system was covered with an outer casing.

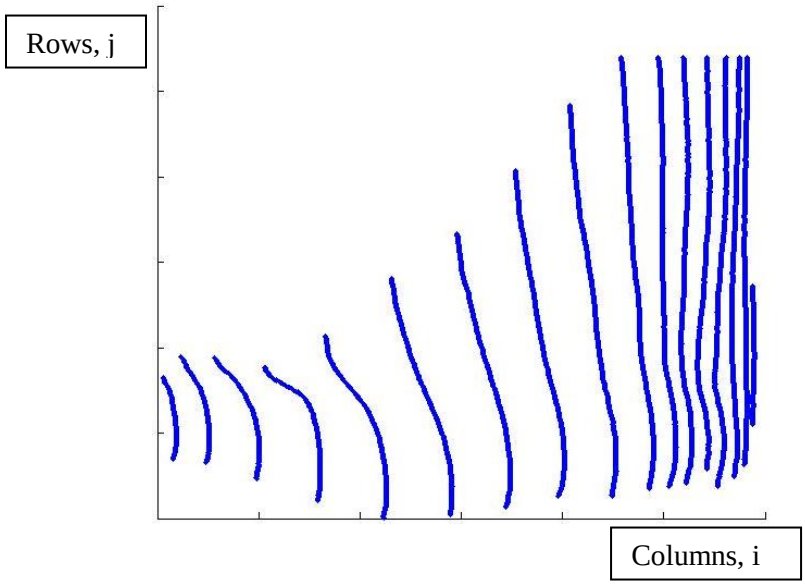

Figure 5-7 Collection of extracted 2D image points from Camera 1 - Sock model (17 images)

A major challenge lies in precisely extracting the set of pixels that represent the foot geometry, leaving out the noise and outliers in the 2D range image. The close range set-up of the optics and varying geometry of the foot posed tough challenges in dealing with the scatter and traces of the laser over the scanner hardware.

5.3 Depth estimation and Post processing 3D data points

The extracted image points (i,j) of the laser are transformed into real-world coordinates based on the mathematical relationship established in section 4.3.2 of this thesis. Section 4.4 explains the computation of mapping the 2D image points of the calibration object to the real world space with the known coefficient matrices. The mapping for foot scan images in 3D space is also established by the same method.

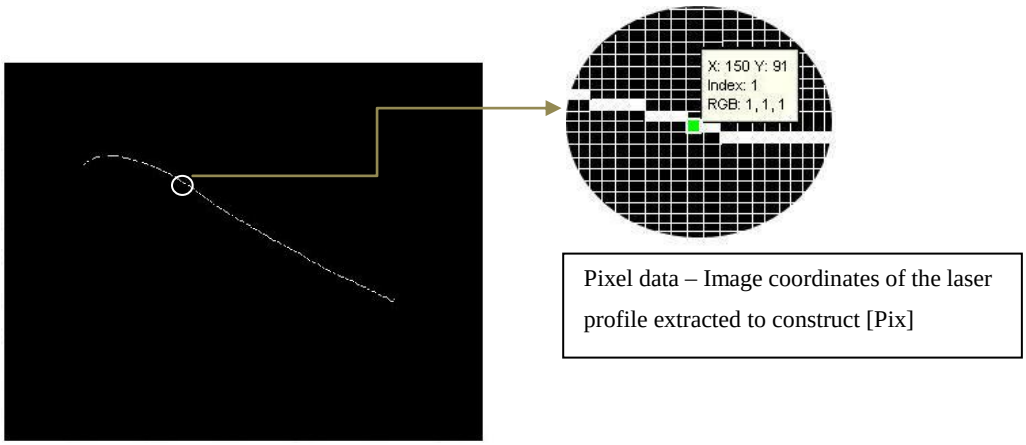

Figure 5-8 Input image coordinates for depth mapping

The image points of the laser stripe are used to construct the $[\mathrm{Pix}]$ matrix. Using the equations transformation is computed for all the 8 cameras independently and the resultant 3D point cloud data is carried over for post processing. Figure 5-8 shows the transformed point cloud data (42750 vertices) from camera1 in range sensor head 1.

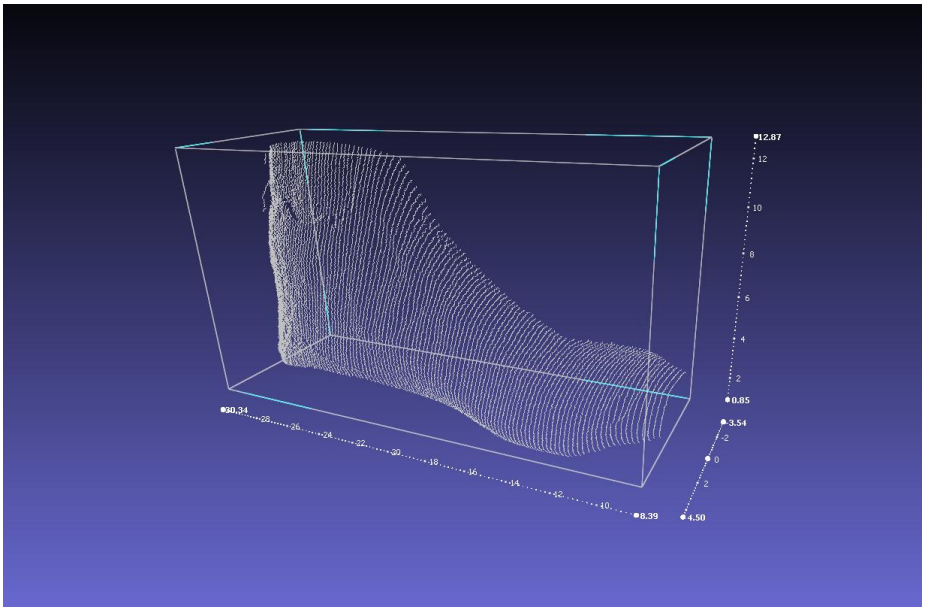

Figure 5-9 3D Point cloud data of camera 1 - Sock model (Viewed in Meshlab environment)

Point cloud data from the 8 cameras were stored as an nx2 Matlab array. Following the depth estimation process, a third level of outlier elimination was carried out. This step was typically carried out to eradicate the 3D points that are found to be extrapolated. The extrapolation in this algorithm happens primarily due to pixel data that lies outside the control volume. Although the image processing algorithms gave the best set of 2D data, it was necessary to have an algorithm to post process the 3D points for more reliability. The algorithm checks for the closest Euclidean distance between consecutive 3D data points and the data points that lie farthest away from the point cloud data are eliminated. Figure 5-9 shows 3D point cloud data with prominent outliers.

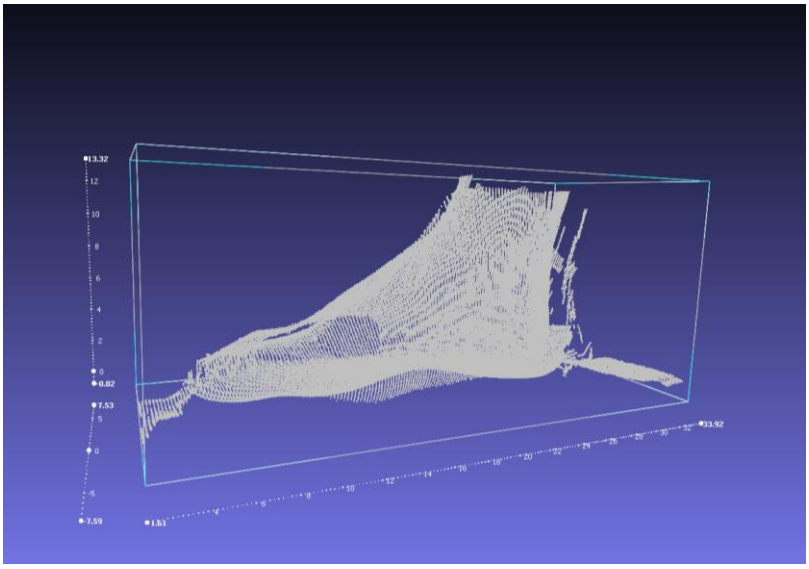

Figure 5-10 3D Point Cloud data with outliers – Viewed in Meshlab environment

On successful elimination, point clouds of all 8 cameras are concatenated into a single array. This array in the range of 50,000 elements represents the digitized foot. The point cloud data of the scanned foot can be easily imported into CAD software as a .ply file. The typical point cloud result of the scanner had 50,000 3D data points representing the scanned foot. The software proved highly advantageous in having a dense point cloud for the low cost set-up.

The .ply format enables high portability of the 3D Data for less memory. So as to obtain the 3D model of the foot, the following operations are carried out.

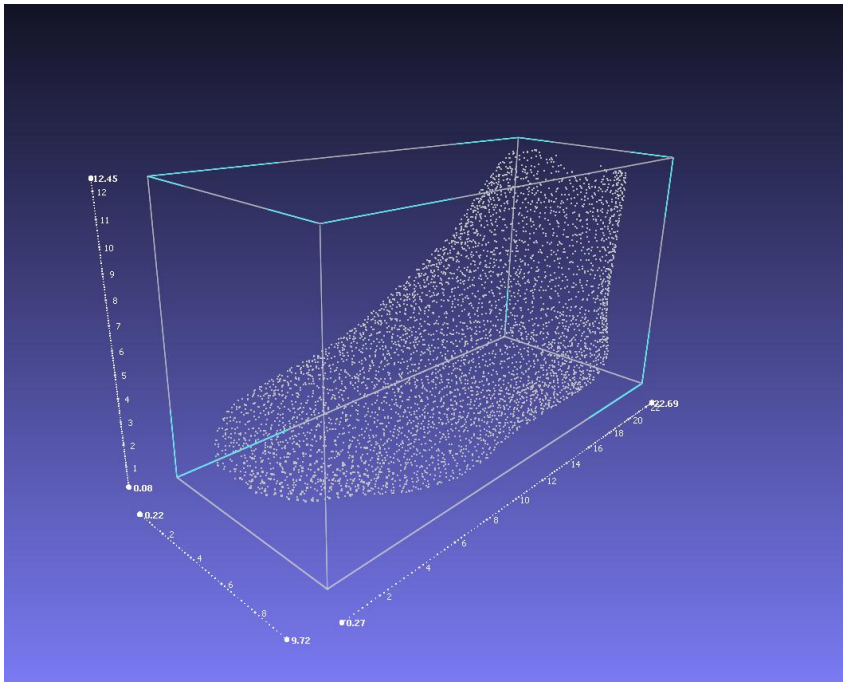

Figure 5-11 3D Point cloud data of the scanned sock model

5.4 CAD model generation

The reconstructed 3D point clouds were created into a mesh that represents the geometry of the scanned object, in this case a human foot. The crust algorithm, developed by Amenta et al. [55] is the most commonly preferred for surface reconstruction. For the given sample of points, the algorithm creates a topologically correct surface with its geometry convergent to that of the original surface. The algorithm mainly relies on Voronoi diagrams and Delaunay triangulation techniques. The Voronoi diagrams help in decomposing a metric space into specific subspaces. The extension of the Voronoi diagram to three dimensions is addressed and proposed workable solutions in the algorithm are discussed in [55].

Delaunay triangulation involves triangulating a surface in such a way that no point on the surface is encapsulated/lies inside the circumcircle of any triangle. This method helps in yielding a triangulated surface with wide triangles (maximizing the minimum angle in the triangle) rather than skinny or

narrower triangles. The extension of Delaunay triangulation involves the use of circumspheres rather circumcircles. The ‘robustcrust’ function developed by Luigi Giaccari based on the ball pivot algorithm [56] is the most preferred for meshing 3D point clouds of a closed surface. A simple and customized function based on ‘robustcrust’ was constructed and implemented to mesh the 3D point cloud data of the foot. Vertices and normals of the triangulated surface are computed in this module.

The next step towards achieving a CAD model is to export the mesh model as a CAD readable format. Standard formats that most CAD software packages and reverse engineering machines like 3D printers accept are .stl or .vrml. The final module of the software focuses on exporting the generated mesh model into a .stl file, which makes it compatible for viewing in CAD software packages and make it more efficient in data transfer.

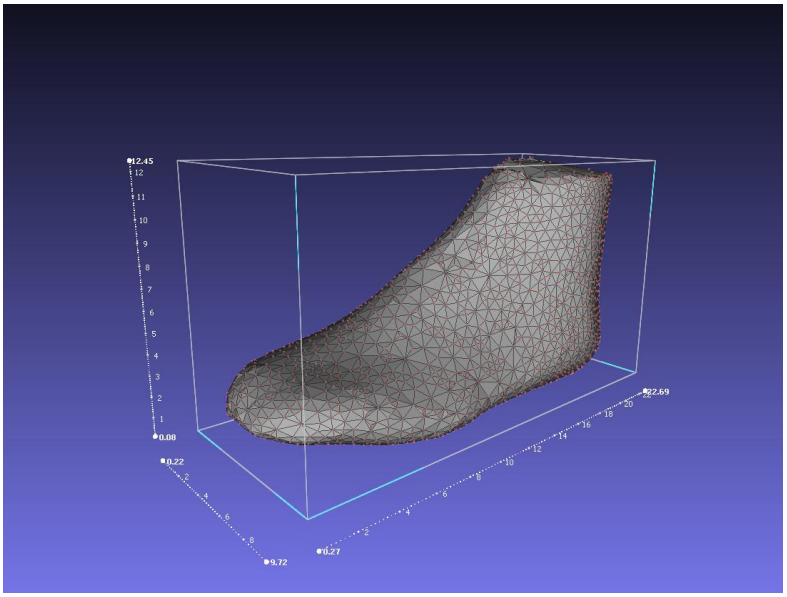

Figure 5-12 Triangulated 3D sock model from the 3D data points

Chapter 6
Performance Verification and Results

This section of thesis documents the results from the scanner and evaluation of the output models in terms of accuracy and precision. Comparison of the 3D foot scanner's result against the scanned result of an Industrial high-end Laser scanner at Northern Digital Inc., [57], was carried out for better analysis. The section also provides an overview of various experiments and trials that were carried out during the calibration process for improved accuracy and precision of the scanner.

6.1 Scan results of Calibration Object

6.1.1 Description

A 3D aluminum block of 15 cm x 10 cm x 5 cm was scanned using the 3D foot scanner to study the accuracy of the scan output model. The block was modeled using Solidworks prior to manufacturing, and its output scan was compared against the CAD model. Figure 6-1 shows some of the key points observed.

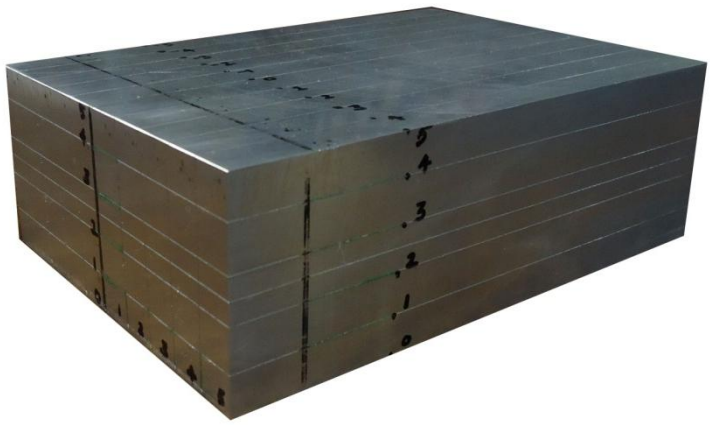

Figure 6-1 Aluminum block (15 x 10 x 5 cm)

6.1.2 Scanner 3D point cloud output

The aluminum block was covered with two layers of mild-yellow colored cloth in order to avoid reflections and scatter of the laser stripe over its surface. The scanner's 3D point cloud output and the reconstructed CAD file were viewed in Meshlab, which are presented in Figure 6-2 and 6-3.

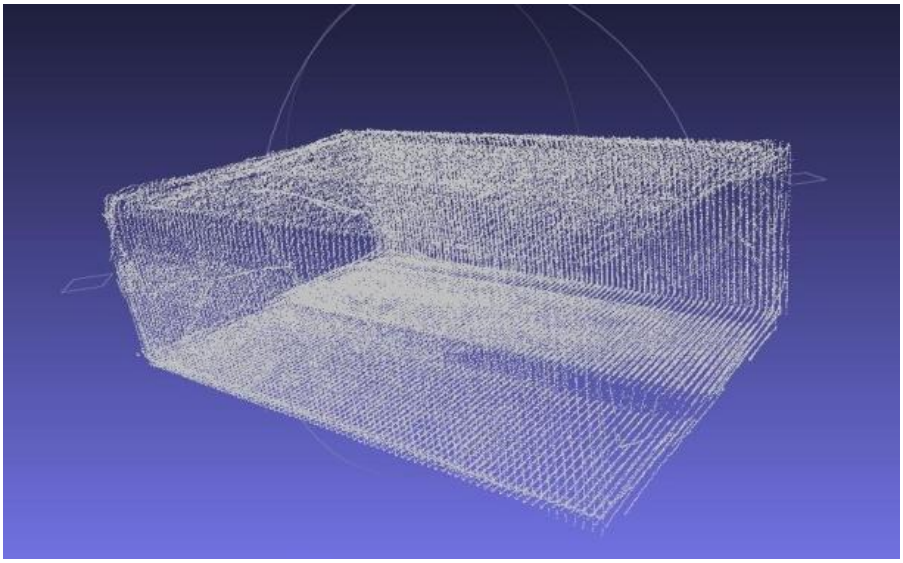

Figure 6-2 3D Point cloud of the block- Viewed in Meshlab

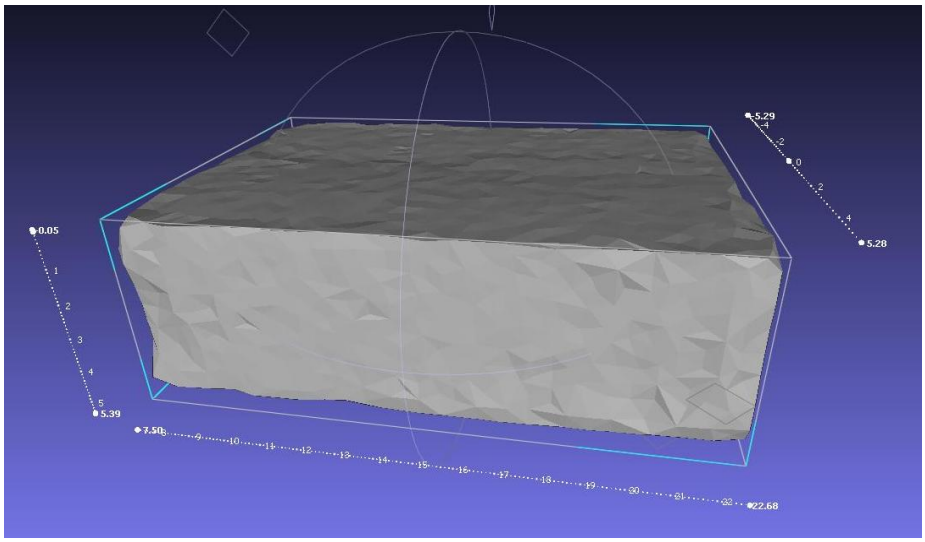

Figure 6-3 Reconstructed block as .stl file - Viewed in Meshlab

6.1.3 Basic dimensional check

A straightforward comparative study of the dimensional differences between the actual CAD model and the scanner generated CAD model was carried out. Table 6-1 shows the deviation in the dimensions between the actual and acquired 3D model. The results show that the scanner could able to generate output models with accuracy of +/-0.05cm.

Table 6-1 Deviations with the actual CAD model and the output CAD model

	Length (cm)	Width (cm)	Height (cm)
Actual CAD model	15	10	5
Scanner CAD model	15.12	10.20	5.14

*The sock material thickness =0.15cm

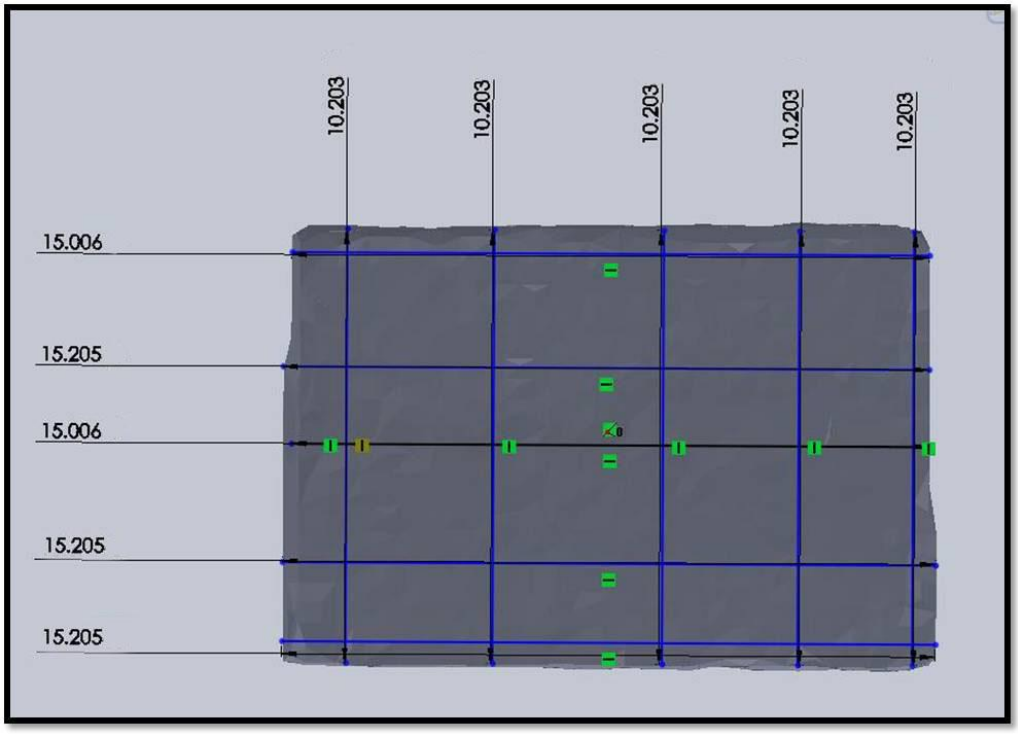

Figure 6-4 Length and width deviation study – Solidworks

6.2 Scan results of Sock model

A sample plaster cast/sock-model of human foot was used for experiments and trials with the scanner. To make a comparative study on the scanner's accuracy, the sock model was scanned with a High-end Industrial laser scanner at NDI, Waterloo [57]. The scanned CAD model was considered to be the reference standard, to validate the foot scanner's performance. Figure 6-5 shows the scanned sock-model from NDI's scanner.

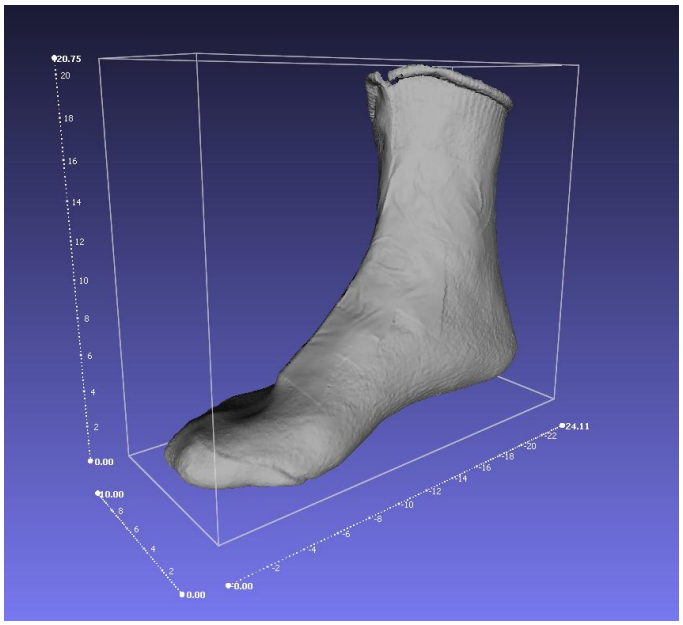

Figure 6-5 Scan result of the Sock model - NDI, Waterloo [57]

The CAD model was highly precise, accurate and featured with high-definition 'texture-mapping'. The sock model was scanned in the 3D foot scanner with a resolution of 0.178cm and a CAD file in .stl file format was generated for comparison with the reference model (shown in Figure 6-6).

6.2.1 Comparison of Foot models by Registration

The comparison between the reference model and the generated model was carried out using open source software called 'CloudCompare' [58], which used point cloud data registration for the purpose of comparing models. Point cloud registration within the software checks for correspondence between

data points by feature matching and by iterative transformations. The software also checks for similarities in surface curvature among the data points and iterates the process until the features/data-points match. Figure 6-7 illustrates the comparison of the two models using 'CloudCompare' [58].

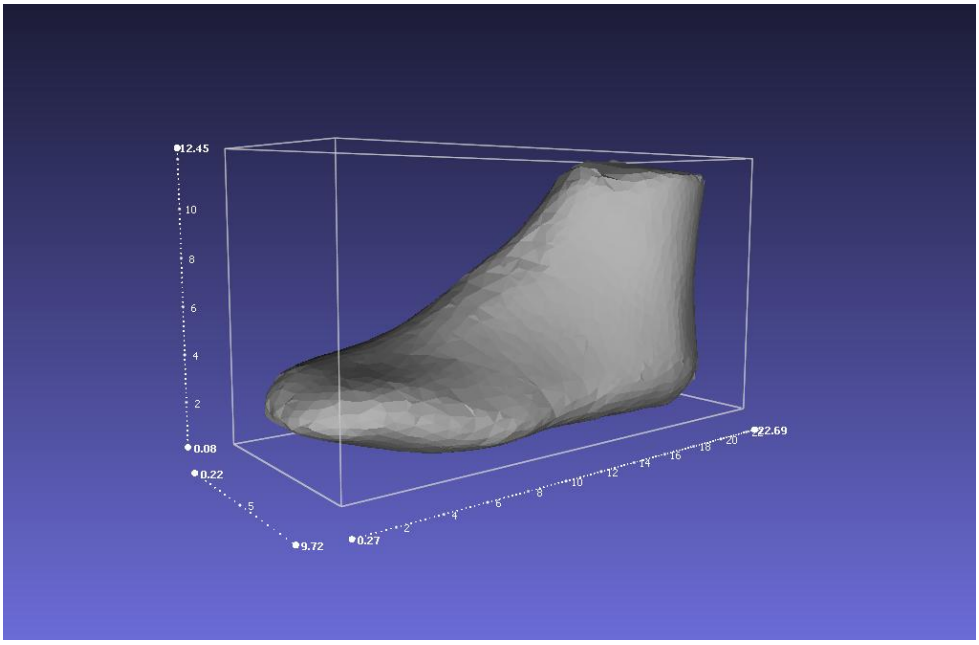

Figure 6-6 Generated 3D .stl file of the Sock model

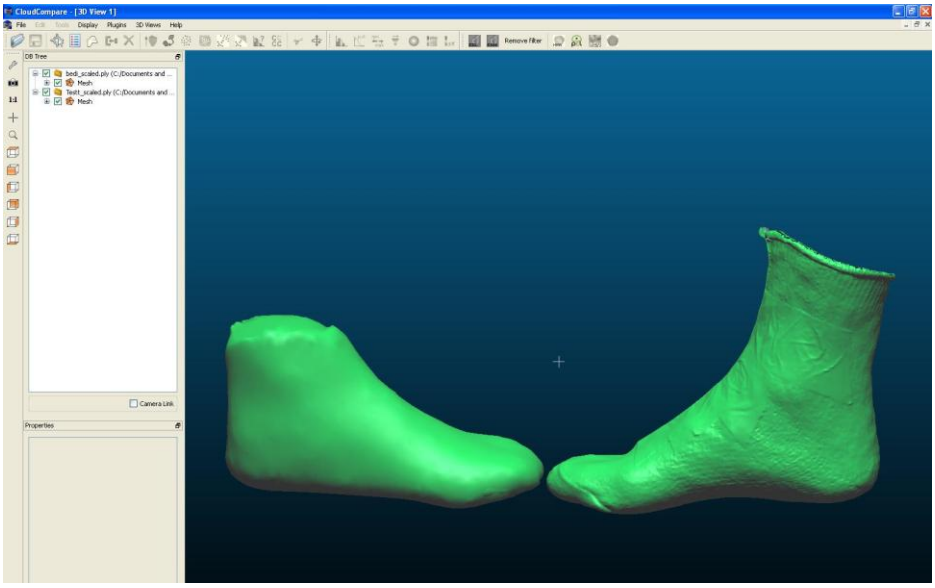

Figure 6-7 Scanner output and reference model – CloudCompare [58] environment

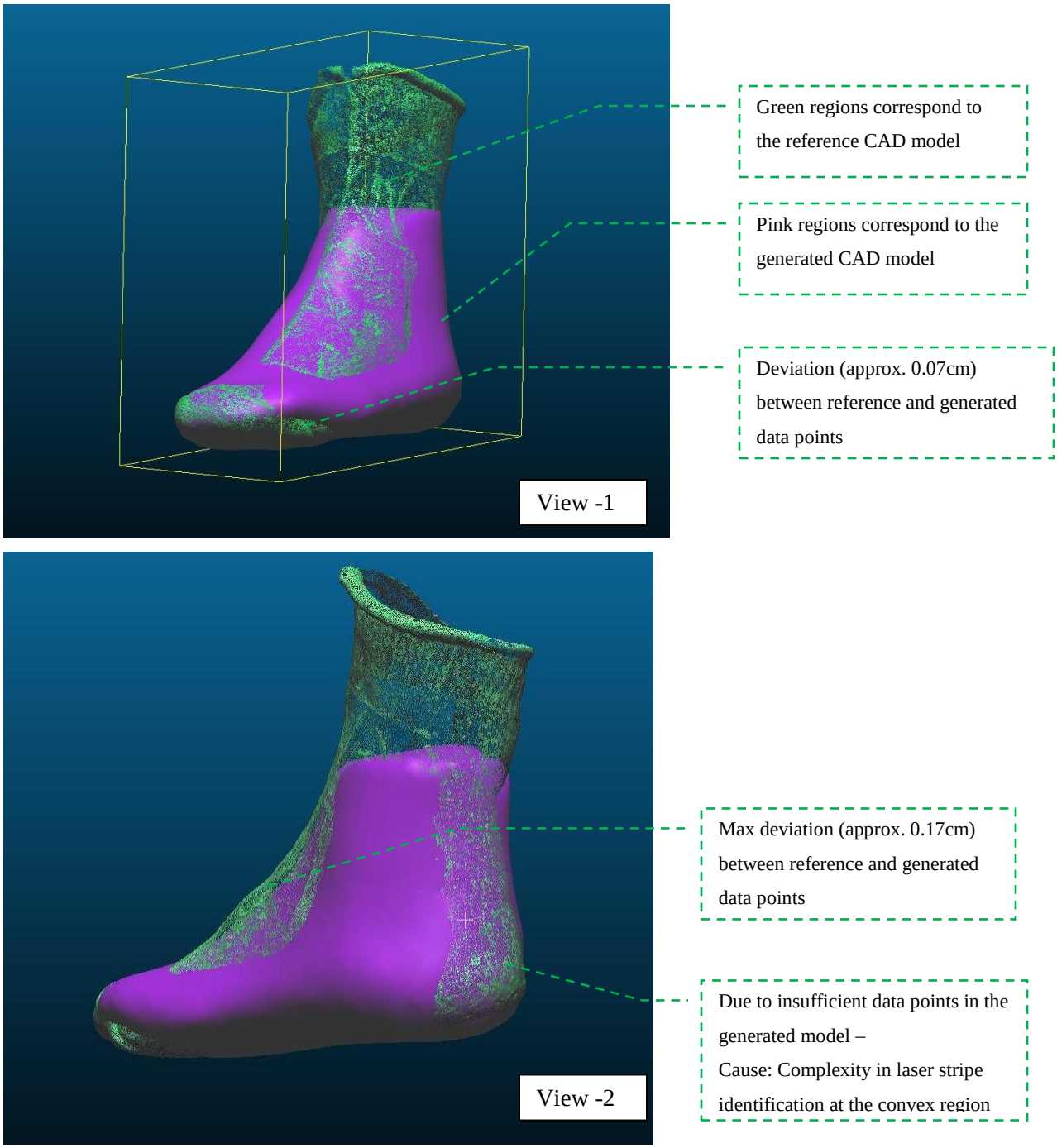

Figure 6-8 Comparison of data points with the reference CAD file- CloudCompare [58] environment

The vertices of the scanner output model were sub-divided into 70 classes based on the distance from its corresponding point in the reference model. The cloud to cloud distance was computed for the models to determine more details on the error in terms of maximum distance, mean distance and standard deviation. Figure 6-9 shows the spread of the data points and their distance from the reference model. 56 classes of the output model's data points were found to be well under 0.1cm (i.e., 80% of the total data points), while the rest found to be under 0.2 cm.

Table 6-2 shows the error based on the cloud to cloud distance comparison. It was found that the maximum distance was 0.310 cm and a mean distance of 0.035 cm.

Figure 6-10 presents the same cloud to cloud distance comparison for 8 classes of the data points.

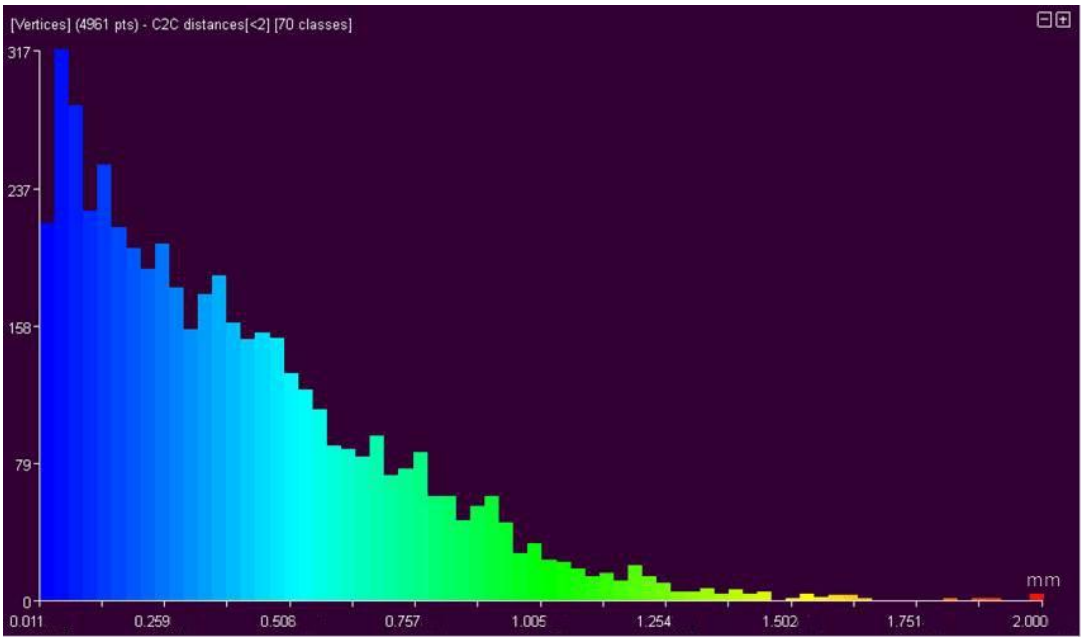

Figure 6-9 Cloud to Cloud distance between reference CAD model and scanner output model

Table 6-2 Results of Cloud to Cloud comparison

Reference	Vertices of Reference CAD model
Compared	Vertices of Scanner Output Model
Minimum Distance (cm)	0
Maximum Distance (cm)	0.31032
Mean Distance (cm)	0.03532
Standard Deviation	0.3075

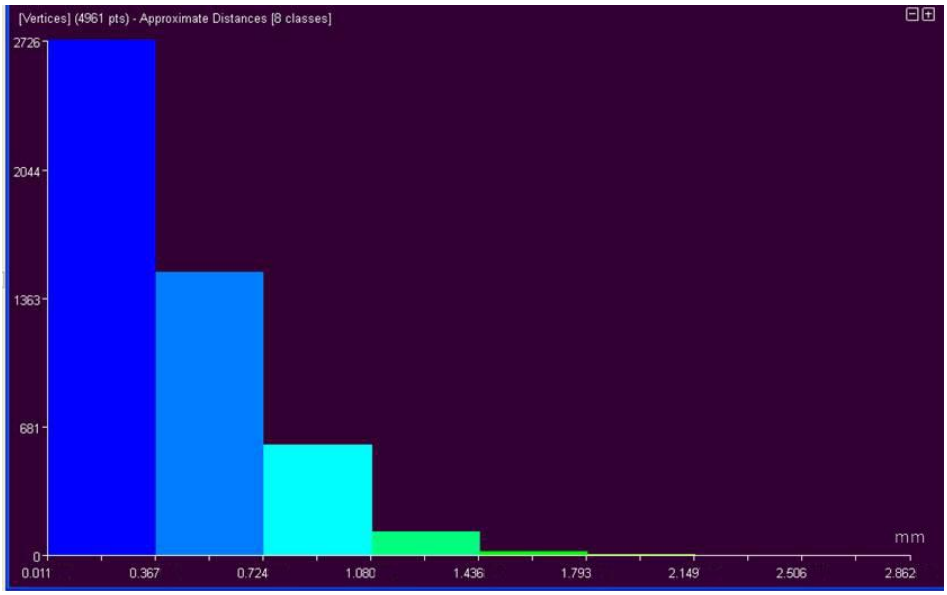

Figure 6-10 Cloud to Cloud distance comparison for 8 classes of data points

6.3 Scan results of human foot

In order to validate the scanner's functionality of scanning a foot, numerous scans were performed with various participants. The scanner was able to successfully generate accurate models of the human feet that differed among various subjects in terms of length, width and girth sizes.

Figure 6-9 presents some of the 3D foot models of the participants.

Figure 6-11 Foot models from the scanner

Chapter 7
Conclusion and Future Work

7.1 Conclusion

Footwear manufacturing integrated with the scanning system is proven to reduce laborious manual measurements and computations. Introduction of 2D scanning systems were effective in achieving accurate information only on the features and the landmarks of a foot. However, it was limited to manufacturing of the orthosis and for measuring basic plantar surface of the foot. On the other hand, 3D foot scanning systems have proven useful for capturing geometry for shoe last manufacturing and for developing custom orthoses and footwear. However, the high cost of current 3D scanning systems makes it unaffordable for many shoemakers and orthotic technicians. The solution for this is a low-cost foot scanner. Digitization and 3D CAD model generation of the foot using such a low-cost structured light scanner was the focus of this thesis.

A technique for optical calibration of the scanner and generation of CAD model was proposed, implemented and tested in this work. The optical setup of the scanner requires calibration to measure the real-world object effectively. The proposed method eliminates the need of complex and laborious computations of the internal and the external parameters of a camera. Added to that, the method is independent of lens distortions and other optical geometry as well, making it highly advantageous. Computations that determine the relationship between 2D image points and 3D real world co-ordinates serve to be memory efficient and possess quicker execution time.

With a computed relationship between the 2D image points and the real world coordinates, the scanner was equipped to generate a 3D model of the foot. The images acquired by the cameras are processed by the image processing script to extract the 2D points of the laser stripe. The image points

are subsequently mapped to their corresponding 3D coordinates. Input images from all the cameras were processed and dense data points representing the scanned foot were obtained.

The 3D data points were triangulated by ball pivoting method to produce a 3D model. The output model consisting of triangles and normals was constructed as a .stl file. This makes the output model to be compliant with any CAD software. The algorithm for image processing and surface reconstruction was tested and comparisons were made between the 3D reference models of known geometry and their corresponding scanner output models. The resolution of the scanner was estimated to be 0.178 cm. The mean error of the scanner's output based on the comparison with the reference sock model was 0.035 cm, which conforms to the target tolerance of less than +/- 0.05 cm. The maximum error of 0.31 cm can be brought down by recalibrating the cameras with more control points. Increasing the number of control points in the calibration process helps in achieving more accurate mapping of 2D image points with the real world data points. The results of the experiments and trials of various foot scans were encouraging and can be expanded in many ways.

7.2 Future Work

The short term objective of the scanner is to interface 8 USB cameras with the processing computer for simultaneous data acquisition. The restricted USB bandwidth is likely to be the cause for this issue. A possible solution for this issue is to loop the USB camera to effectively use the bandwidth and also trials are being carried out using advanced Peripheral Component Interconnect (PCI) card to interface USB ports with the computer. In addition to this, trials are being carried out using pinhole camera-laser setup, to improve the quality of input scan images.

The long term objective of the scanner includes sizing, texture mapping and landmark detections based on the generated 3D CAD model of the foot. Sizing is the most common requirement during a footwear purchase. It can be estimated by measuring the basic geometries mentioned in Chapter 2

from the CAD model. Mondopoint is a well-known shoe sizing system which is preferred by the footwear industry professionals for sizing measurements. This system involves the estimation of the mean foot length and width of the foot which can be acquired through the measurable 3D CAD model from the scanner. The sizing module could be incorporated into the surface reconstruction module so that sizing measurements are achieved along with the CAD file. Similarly, incorporation of texture mapping features in the CAD model would add the credibility of the scanner in terms of feature detection, landmark identification and other clinical purposes.

Improvements in the calibration process in terms of (i) increasing the control points on the reference object, (ii) ensuring higher order of control point measurement accuracy (to be greater than the target accuracy of the scanner), and (iii) uniform distribution of control points over the scan volume would serve to be a good starting point for any further experiments and trials.

Appendix A

Estimation of Goodness of Fit

Estimation of R^2 to determine the total variation of 'Y' and 'Z' for the variations in the input data (i,j): Y_{obs} and Z_{obs} are computed from the known image coordinates i, j and the coefficient matrix by equations 4.12 and 4.13. With the known actual data and the observed data, R^2 can be computed as follows.

$$R^2_{y,z} = 1 - \frac{SE_{y,z}}{SV_{y,z}}$$

The squared errors $SE_{y,z}$ can be determined by,

$$SE_y = (Y_{act} - Y_{obs})^2$$

$$SE_z = (Z_{act} - Z_{obs})^2$$

And the Squared variations $SV_{y,z}$ can be determined by,

$$SV_y = (Y_{act} - Mean_Y)^2$$

$$SV_z = (Z_{act} - Mean_Z)^2$$

The following table is computed based on the above formula and the value of R^2 is achieved.

Inputs		**Actual 'Y'** Y_{act}	**Observed 'Y'** Y_{obs}	**Squared Error** SE_y	**Squared Variation** SV_y
i	**j**				
159	221	5	4.9032	0.009	6.76
318	170	5	4.6643	0.113	6.76
397	225	2	1.4752	0.275	0.16
530	192	2	1.0706	0.864	0.16
591	255	-2	-3.1572	1.339	19.36
$Mean_Y$		2.4	**Total**	ΣSE_Y = 2.6	ΣSV_Y = 33.2

Percentage of variation, not explained by the variations in input:

$$= \frac{\Sigma SE_Y}{\Sigma SV_Y} = \frac{2.6}{33.2} = 0.0783 = 7.83\%$$

Therefore, the percentage of total variations of 'Y' values explained by the variations in input can be estimated as,

$$R^2_Y = 1 - 0.0783 = 0.9217 = 92.17\%$$

Similarly, for estimating the goodness of the equation relating to 'Z' can be determined as,

Inputs		**Actual 'Z'** Z_{act}	**Observed 'Z'** Z_{obs}	**Squared Error** SE_Z	**Squared Variation** SV_z
i	**j**				
159	221	3	3.0000	0	19.36
318	170	7	6.9999	0	0.16
397	225	7	7.0000	0	0.16
530	192	10	10.0000	0	6.76
591	255	10	9.9999	0	6.76
$Mean_z$		7.4	**Total**	$\Sigma SE_z = 0$	$\Sigma SV_Z = 33.2$

Percentage of variation, not explained by the variations in input:

$$= \frac{\Sigma SE_Z}{\Sigma SV_Z} = \frac{0}{33.2} = 0 = 0\ \%$$

Therefore, the percentage of total variations of 'Z' values explained by the variations in input can be estimated as,

$$R^2_z = 1 - 0 = 1 = 100\ \%$$

It was found that, Y_{obs} and Z_{obs} varies with the increase in the significant digits of non-zero values in the coefficients α_y and α_z respectively. The above computations were carried out with 5 significant figures. Results may vary for computations with any significant digit greater than 5.

Appendix B

Calibration Chart for 8 Cameras

Consolidated Chart of Coefficients – Result of Camera Calibration Process

Camera 1

Real world		Image Point		Resultant Co-Efficients	
Y	Z	i	j	$[\alpha_y]$	$[\alpha_z]$
3	5	159	221	0.000	0.000
7	5	318	170	-0.022	-0.009
7	2	397	225	0.138	0.082
10	2	530	192	0.000	0.000
10	-2	591	255	0.000	0.000
				0.000	0.000

Camera 2

Real world		Image Point		Resultant Co-Efficients	
Y	Z	i	j	$[\alpha_y]$	$[\alpha_z]$
3	5	550	217	0.000	0.000
7	5	389	170	0.009	0.002
7	2	311	228	0.041	0.119
10	2	176	196	0.000	0.000
10	-2	113	261	0.000	0.000
				0.000	0.000

Camera 3

Real world		Image Point		Resultant Co-Efficients	
Y	Z	i	j	$[\alpha_y]$	$[\alpha_z]$
3	-5	570	244	0.000	0.000
7	-5	413	204	-0.008	0.003
7	-2	340	252	-0.048	0.111
10	-2	207	227	0.000	0.000
10	2	147	287	0.000	0.000
				0.000	0.000

Camera 4

Real world		Image Point		Resultant Co-Efficients	
Y	Z	i	j	$[\alpha_y]$	$[\alpha_z]$
3	-5	143	231	0.000	0.000
7	-5	303	188	0.015	-0.008
7	-2	377	238	-0.121	0.077
10	-2	502	206	0.000	0.000
10	2	559	265	0.000	0.000
				0.000	0.000

Camera 5

Real world		Image Point		Resultant Co-Efficients	
Y	Z	i	j	$[\alpha_y]$	$[\alpha_z]$
0	-2	60	222	0.000	0.000
0	2	287	130	0.005	-0.005
3	2	411	245	0.004	-0.009
3	5	591	178	0.000	0.000
6	5	640	255	0.000	0.000
				0.000	0.000

Camera 6

Real world		Image Point		Resultant Co-Efficients	
Y	Z	i	j	$[\alpha_y]$	$[\alpha_z]$
0	-2	605	270	0.000	0.000
0	2	388	186	0.001	-0.005
3	2	279	303	0.045	0.008
3	5	93	247	0.000	0.000
7	5	9	386	0.000	0.000
				0.000	0.000

Camera 7

Real world		Image Point		Resultant Co-Efficients	
Y	Z	i	j	$[\alpha_y]$	$[\alpha_z]$
0	2	64	35	0.000	0.000
0	-2	288	118	-0.001	0.007
3	-2	400	6	0.085	-0.012
3	-5	581	62	0.000	0.000
5	-5	622	2	0.000	0.000
				-0.001	0.000

Camera 8

Real world		Image Point		Resultant Co-Efficients	
Y	Z	i	j	$[\alpha_y]$	$[\alpha_z]$
0	2	640	112	0.000	0.000
0	-2	442	192	-0.090	0.126
3	-2	330	74	0.263	-0.381
3	-5	143	132	0.000	0.000
7	-5	58	1	0.001	-0.001
				-0.003	0.004

References

[1] S. J. Lochner, *Automation of shoe last modification and tool path planning,* Waterloo: University of Waterloo, 2009.

[2] D. Besliu, *Measurement Devices for Custom Shoe Manufacturing,* Waterloo: University of Waterloo, 2011.

[3] S. Telfer and J. Woodburn, "The use of 3D surface scanning for the measurement and assessment of human foot," *Journal of foot and ankle research,* no. 10.1186/1757-1146-3-19, p. 3:19, 2010.

[4] T. B. D. Company, "The Brannock Device Co., Inc.," [Online]. Available: http://brannock.com/brannock/images/brannock2.jpg. [Accessed 5 11 2012].

[5] C. Witana, S. Xiong, J. Zhao and R. Goonetilleke, "Foot measurements from 3 Dimensional scans; a comparison and evaluation of different methods," *Int J Ind Ergon,* pp. 36:789-807, 2006.

[6] X. Liu, W. Kim and B. Drerup, "3D characterization and localization of anatomical landmarks of the foot by FastSCAN," *Realtime Imaging,* pp. 10:217-228, 2004.

[7] I. Krauss, S. Grau, M. Mauch, C. Maiwald and T. Horstmann, "Sex-related differences in foot shape.," *Ergonomics,* pp. 51:1693-1709, 2008.

[8] Lou G, Houston VL, Mussman M, Garbarini M, Beattie AC and Thongpop C, "Comparison of male and female foot shape," *J Am Podiat Med Assoc,* pp. 99:383-390, 2009.

[9] Wunderlich RE and Cavanagh PR, "Gender differences in adult foot shape; Implications for shoe design," *Med Sci Sports Exerc,* pp. 33:605-11, 2001.

[10] Bao HP, Soundar P and Yang T, "Integrated approach to design and manufacture of shoe lasts for orthopeadic use," *Comput Eng,* pp. 26:411-421, 1994.

[11] Nacher B, Alemany S, Gonzalez JC, Alcantara E, Garcia-Hernandez J, Heras S and Juan A, "A foot wear fit classification model based on anthropometric data," in *8th annual digital human modelling for design and engineering symposium,* Lyon, 2006.

[12] Wang C-S, "An analysis and evaluation of fitness for shoe lasts and human feet," *Comput Ind,* pp. 61:532-540, 2010.

[13] Hawke F, Burns J, Radford JA and du Toit V, "Custom made foot orthotics for the treatment of foot pain," *Cochrane Database system Rev,* p. 16:CD006801, 2008.

[14] Guldemond NA, Leffers P, Sanders AP, Emmen H, Schaper NC and Walenkamp GHIM, "Casting methods and plantar pressure: effects of custom made foot orthoses on dynamic plantar pressure distribution," *J Am Pod Med Assoc,* pp. 96:9-18, 2006.

[15] Coudert T, Vacher P, Smits C and Van Der Zande M, "A method to obtain 3D foot shape deformation during the GAIT cycle," in *9th international symposium on the 3d analysis of human movement*, Valenciennes, June 2006.

[16] Kimura M, Mochimaru M and Kanade T, "3D measurement of feature cross-sections of foot while walking," *Mach Vis Appl.*

[17] Jezerek M and Mozina J, "High-speed measurement of foot shape based on multiple-laser-plane triangulation," *Opt Eng,* p. 48:113604, 2009.

[18] F. Chen, G. M. Brown and M. Song, "Overview of three-dimensional shape measurement using optical methods," *Optical Engineering,* vol. 39, no. 1, pp. 293-312, 2000.

[19] Blais F, Bisson J.A, Williams S, Roberston N, Rozin S and Nelson A, "The ShapeGrabber FootScanner: a low cost high accuracy 3D system for the acquisition of human feet," *The International society of Optical Engineering,* vol. 3958, pp. 178-186, 2000.

[20] Kouchi M and Mochimaru M, "Development of a Low-cost footscanner foe a custom shoe making system," in *Proceedings of the 5th symposium on footwear boimechanics*, Zuerich, 2001.

[21] Leon Kos, "A system for footwear fitting analysis," *International design conference,* pp. 1187-1192.

[22] H.J.Tiziani, "Optical metrology of engineering surfaces-scope and trends," *Optical measurement techniques and applications,* 1997.

[23] I.Moring, H.Ailisto, V.Koivunen and R.Myllyla, "Active vision ssystem for automatic model-based shape inspection," *Opt. Laser Eng.,* vol. 10, pp. 3-4, 1989.

[24] J.Y.Wang, "Imaging laser radar - an overview," in *Processdings of 9th international conference Laser,* 1986.

[25] J.C.Marron and T.J.Schulz, "Three dimensional, fine resolution imaging using laser frequency diversity," *Opt. Lett,* vol. 17, pp. 285-287, 1992.

[26] J.C.Marron and K.S.Schroeder, "Three dimensional lensless imaging using laser frequency diversity," *Appl. Opt.*, vol. 31, pp. 255-262, 1992.

[27] H.Takasaki, "Moire topography," *Appl. opt*, vol. 9, pp. 1467-1472, 1970.

[28] R.Harding and R.Tait, "Moire technique applied to automated inspection of machine parts," in *Proceedings SME vision*, Detroit, 1986.

[29] A.Asundi, "Computer Aided Moire methods," *Opt. Lasers Eng.*, vol. 17, pp. 107-116, 1993.

[30] C.M.Wong, "Image processing in experimental mechanics," *M.Phil thesis, University of Hong Kong*, 1993.

[31] K.Bieman and K.Harding, "3D imaging using a unique refractive optic design to combine moire and stereo," in *Proceedings SPIE*, 1997.

[32] E.Dalhoff, E.Fischer, S.Kreuz and H.J.Tiziani, "Double hetrodyne interferometry for high precision distance measurements," in *Proceeding SPIE*, 1993.

[33] J.D.Trolinger, "Ultra-high resolution interferometry," in *Proceedings SPIE*, 1996.

[34] W.Wester-Ebbinghaus, "Analytics in non-topographic photogrametry," *ISPRS Cong., Com.v., Kyoto*, pp. 380-390, 1988.

[35] C.S.Fraser, "Photogrammetric measurement to one part in a million," *Phtogramm. Eng Remote sens*, vol. 58, no. 3, pp. 305-310, 1992.

[36] E.Muller, "Fast three dimensional form measurement system," *Opt.Eng*, vol. 34, no. 9, pp. 2754-2756, 1995.

[37] Z.Ji and M.C.Leu, "Design of optical triangulation devices," *Opt. Laser Technol.*, vol. 21, no. 5, pp. 335-338, 1989.

[38] C.P.Keferstein and M.Marxer, "Testing bench for laser triangulation sensors," *Sens. Rev*, vol. 18, no. 3, pp. 183-187, 1998.

[39] M.Idesawa, "High precision image position sensing methods suitable for 3D measurements," *Opt.Laser.Eng*, vol. 10, pp. 3-4, 1989.

[40] Zhengyou Zhang, "A flexible new technique for camera calibration," *IEEE transactions on pattern analysis and machine intelligence*, vol. 22, no. 11, pp. 1330-1334, 2000.

[41] C. Y.-l. Liu, *Three-dimensional Hand tracking and Surface geometry measurement for a robot-vision system*, Thesis, University of Waterloo, 2008.

[42] J. Kofman, *SYDE 625 computer vision and 3D Imaging,* Graduate Course notes, 2012.

[43] T. Clarke and J. Fryer, "The Development of Camera Calibration Methods and Models," *The Photogrammetric Record,* vol. 16, no. 92, pp. 293-312, 1998.

[44] J. Heikkila and O. Silven, "A four step calibration procedure with implicit image correction," *IEEE computer society conference on computer vision and Pattern recognition,* 1997.

[45] T. B, "Autocalibration from planar scenes," *ECCV,* pp. 89-105, 1998.

[46] R. Tsai, "A versatile camera calibration technique for high-accuracy 3D machine vision metrology using the off-shelf TV cameras and lenses," *IEEE journal of Robotics and Automation,* vol. 3, no. 4, 1987.

[47] O.Faugeras, Three Dimensional Computer Vision: a geometric viewpoint, MIT Press, 1993.

[48] K. Levenberg, "A method for the solution of certain problems in least squares," *Quart.Appl.Math,* vol. 2, pp. 164-168, 1994.

[49] D. Marquardt, "An algorithm for least squares estimation of non-linear parameters.," *SIAM J.Appl.Math,* vol. 11, pp. 431-441, 1963.

[50] A.Yokoyama, K.Sato, T.Yoshigahara and S.Inokuchi, "Realtime range imaging using adjustment free photo vlsi," in *Proceedings of the IEEE/RSJ International conference on Intelligent robots and systems,* 1994.

[51] J. Forest and J. Salvi, "A review of laser scanning three-dimensional digitisers," in *Proceedings of the IEEE/RSJ International Conference on Intelligent robots and systems*, Switzerland, 2002.

[52] Xiaoyang Yu, Jian Zhang, Liying Wu and Xifu Qiang, "Laser scanning device used in space encoding rangefinder," *Automated opt. Insp. for Industy, SPIE,* pp. 490-495, 1996.

[53] Kazuyuki Hattori and Yukio Sato, "Handy rangefinder for active vision," *In proceedings of IEEE Int;. Conf on Robotics and Automation,* pp. 1423-1428, 1995.

[54] Kazuo Araki, Yukio Sato and Srinivasan Parthasarathy, "High Speed rangefinder," *In SPIE Editor, Optics, Illumination and Image sensing,* vol. 850, pp. 184-188, 1987.

[55] N Amenta, S.Choi and R.Kolluri, "The Power Crust," in *ACM Symposium on Solid Modelling and Applications,* 2001.

[56] Fausto Bernardini; Joshua Mittleman; Holly Rushmeier; Claudio Silva; Gabriel Taubin;, "The Ball-Pivoting algorithm for Surface Reconstruction," *IBM Journal of Research and*

Development.

[57] "Accurate Measurement Solutions for Industrial and Life Sciences Applications," NDI, [Online]. Available: http://www.ndigital.com/. [Accessed 21 11 2012].

[58] "CloudCompare - Open source Project," [Online]. Available: http://www.danielgm.net/cc/. [Accessed 21 11 2012].